Biocatalytic Nanomaterials: A New Pathway for Bacterial Disinfection

Xin Fan, Fan Yang, Chuanxiong Nie, Lang Ma, Chong Cheng,* and Rainer Haag**

Clinical treatment of pathogenic infection has emerged as a growing challenge in global public health. Such treatment is currently limited to antibiotics, but abuse of antibiotics have induced multidrug resistance and high fatality rates in anti-infection therapies. Thus, it is vital to develop alternative bactericidal agents to open novel disinfection pathways. Drawing inspiration from elements of the human immune system that show great potential for controlling pathogens or regulating cell apoptosis, the design of biocatalytic nanomaterials (BCNs) have provided unrivaled opportunities for future antibacterial therapies. More significantly, BCNs exhibit various superior properties to immune cells and natural enzymes, such as higher biocatalytic performance, extraordinary stability against harsh conditions, and scalable production. In this review, the most recent efforts toward developing BCN-based biomedical applications in combating bacterial infections are focused upon. BCNs' antibacterial mechanisms, the classification of BCNs, antibacterial activities that can be triggered or augmented by energy conversion, and the eradication of biofilms with BCNs are systematically introduced and discussed. The current challenges and prospects of BCNs for biocatalytic disinfection are also summarized. It is anticipated this review will provide new therapeutic insights into combating bacteria and biofilms and offer significant new inspiration for designing future biocatalytic nanomaterials.

X. Fan, Dr. C. Nie, Prof. R. Haag
Department of Chemistry and Biochemistry
Freie Universität Berlin
Takustraße 3, 14195 Berlin, Germany
E-mail: haag@zedat.fu-berlin.de
F. Yang, Prof. L. Ma, Prof. C. Cheng
College of Polymer Science and Engineering
Department of Ultrasound, West China Hospital
Sichuan University
Yihuan Road No. 24, Chengdu 610065, China
E-mail: malang1989@scu.edu.cn; chong.cheng@scu.edu.cn
F. Yang
Department of Physics
Freie Universität Berlin
Arnimallee 14, 14195 Berlin, Germany
Prof. C. Cheng
State Key Laboratory of Polymer Materials Engineering
Sichuan University
Chengdu 610064, China

The ORCID identification number(s) for the author(s) of this article can be found under https://doi.org/10.1002/adma.202100637.

1. Introduction

Bacterial infectious diseases have emerged as a major global health problem. With the discovery of antibiotics like penicillin, it was once thought that bacterial infections would be cured forever. Unfortunately, the abuse and misapplication of antibiotics over decades has aroused the evolutionary potential of bacteria, triggering the generation of more robust strains with multidrug resistance.[1] Once such bacteria have coalesced into a biofilm, their drug resistance will be even stronger. This is because the extracellular polymeric substances (EPSs), which are biofilms' major components and are responsible for maintaining their structure and metabolism, will serve as strict guard, preventing permeation by antimicrobials. It is therefore urgent to develop new agents to deal with the growing problem of bacterial infections. With the rapid development of nanotechnology, researchers have proposed numerous valuable concepts for the construction of antibacterial and anti-biofilm platforms, which can be briefly classified as follows: 1) nanostructures loaded with biocides, antimicrobial peptides,[2] and other bactericidal components;[3–5] 2) nanostructures that show intrinsic bactericidal activity by means of imposing chemical or physical damage on bacteria, such as silver nanoparticles, titanium dioxide, and nano-sized zinc oxide;[6–11] 3) nanostructures that can generate photothermal effects when activated by near-infrared light (NIR);[12–14] 4) nanostructures that can produce massive amounts of reactive oxygen species (ROS) with peroxide or photo-/sono-stimulation; and 5) combining two or more bactericidal components or modalities to synergetically optimize treatment efficacy.[15,16]

Up to now, a variety of nanostructured platforms have been developed for combating bacteria and their biofilm.[17–19] Although most of them exhibited acceptable disinfection outcomes, they still face a series of fatal flaws like narrow-spectrum antibacterial performance, damaging only certain bacterial components, low bactericidal efficiency, non-localized or nonspecific toxicity, and poor long-term physiological stability. Taking the extensively studied silver nanocomposites as an example, although they have been demonstrated to induce a broad-spectrum inactivation of bacteria/biofilm,[12] their excessive and nonspecific toxicity poses a potential threat to healthy

cells and tissues, placing a formidable limitation on in vivo therapies.[20] Furthermore, it is difficult to maintain long-term antimicrobial activity with this ion-release bactericidal mechanism. Hence, it is urgent to develop safer and more efficient strategies to overcome the current obstacles to traditional nanomaterials-based antibacterial therapies.

The human immune system shows great power in fighting pathogens and regulating cell apoptosis via the biocatalytic generation of ROS. For instance, the peroxidase (POD) from lysosomes and neutrophils can catalyze hydrogen peroxide (H_2O_2) to generate hydroxyl radicals ($\cdot OH$), which can inflict serious oxidative damage on pathogens.[21,22] Nevertheless, it is not practical to directly use natural enzymes as antimicrobials owing to their intrinsic disadvantages, such as high production cost, complicated purification, and poor stability. Therefore, in order to construct a cost-effective biocatalytic antibacterial/antibiofilm nanoplatform, recently, researchers have strived to develop metal-based, carbon-based, and polymer-based biocatalytic nanomaterials, or BCNs, that is, nanomaterials with catalytic performance inspired by or similar to biological enzymes.[23–36] These BCNs are reported to exhibit various advantages, such as tunable composition and catalytic activity, very limited cytotoxicity in appropriate dosages, remarkable stability, and unique energy-conversion ability, which make them ideal candidates for bacterial disinfection therapies.

Benefiting from their superior physiochemical properties, BCNs have become an essential and well-traveled investigation area, with efforts directed to the design and fabrication of BCNs with unique potential for future antibacterial therapies.[37–39] To provide a timely summary of this rapidly growing field, this review will focus on the most recent efforts toward developing BCNs to serve as a new pathway for disinfection therapies in combating bacterial infections. We will systematically introduce and thoroughly discuss BCNs' antibacterial mechanisms; the classification of BCNs; antibacterial activities that can be triggered or augmented by energy conversion; and the eradication of biofilms with BCNs. We will also summarize in depth the current challenges and prospects of BCNs for biocatalytic disinfection. We anticipate that this review will provide new insights into developing BCNs as novel antibacterial agents for combating bacteria and biofilms and offer significant new inspiration for designing future biocatalytic nanoagents for clinical and industrial applications.

## 2. Design and Fabrication of ROS Catalytic Nanomedicines for Combating Bacteria/Biofilms

In the following sections, we will first discuss the different antibacterial mechanisms of BCNs. We will then discuss various BCN design and fabrication strategies, such as self-catalyzed BCNs or hybrid BCNs with encapsulated natural enzymes as ROS generators for killing bacteria. Next we will classify and comprehensively discuss BCNs with POD-mimetic, glucose oxidase (GOx)-assisted, GOx-mimetic, and haloperoxidase (HPO)-mimetic activities. These BCNs are being investigated to increase bactericidal efficacy and decrease the toxicity induced by overdosage of traditional disinfection chemical auxiliaries like H_2O_2. Third, we will discuss

energy-dependent BCNs whose catalytic performance can be activated or significantly augmented by introducing extra energy sources such as visible light, laser, or ultrasound; such BCNs promise the ability to devise controllable on-demand bactericidal modalities. Fourth, we will summarize BCNs with autoinducer quenching activity to disrupt quorum sensing, as well as BCNs with extracellular DNA (eDNA) cleavage activity; these BCNs target the critical roles in the establishment and integrity of biofilms. Next, we will further discuss current biofilm microenvironment-responsive BCN-based systems, which can employ characteristics of the biofilm microenvironment (BME) as coadjutant for highly efficient and specific biofilm eradication. Finally, we will summarize in depth and comment on the current challenges and prospects of BCNs for biocatalytic disinfection.

2.1. Detailed Antibacterial Mechanisms of BCNs

Up to now, numerous different types of BCNs have been designed and reported to exhibit intrinsic abilities in killing bacteria or eradicating biofilm. The mechanisms of BCNs' robust bactericidal activities can be divided into the following areas, as illustrated in **Scheme 1**.

1) Redox BCNs show intrinsic ROS generation capability. For example, oxidase-mimetic nanocatalysts can catalyze oxygen to produce $\cdot O_2^-$, which can nonselectively destroy bacteria and biofilm by denaturing their proteins, membrane lipids, or DNA. Since these BCNs can cause bacterial cellular damage at both genetic and structural levels, bacteria can hardly develop resistance to them.[45]

2) Some BCNs are capable of generating ROS without extra energy input upon the addition of chemical auxiliaries.[46,47] For example, H_2O_2 is regarded as a general disinfection agent. However, to achieve satisfying antibacterial outcomes in wound treatment, a high concentration of H_2O_2 (up to 3%) is usually required,[48] which is too high for healthy tissues nearby.[48] Thankfully, the POD-mimetic nanocatalysts can catalyze H_2O_2 to the strongly oxidative $\cdot OH$,[49,50] thus minimizing the dosage of H_2O_2 during the therapeutic process. Furthermore, HPO-mimetic nanocatalysts can generate abundant ROSs, like hypohalous acid and $^1O_2$, in the presence of both H_2O_2 and halogen ions; these ROSs can destroy bacteria and even their biofilms.[51] While the H_2O_2-dependent BCN-based therapy often tends to show high pH dependence, the dosage of ex situ H_2O_2 is relatively high, resulting in limited antibacterial efficiency with undesired damage to normal tissues.[52,53] Therefore, researchers have recently encapsulated GOx and GOx mimetics inside POD mimetics as potential candidates for antibacterial and antibiofilm therapies. In the presence of glucose, GOx can generate H_2O_2 in situ, which the POD mimetic can then catalyze to the ROS $\cdot OH$. If POD mimetics contain encapsulated GOx or have GOx-mimetic components, they may achieve a cascade catalytic reaction from glucose to H_2O_2 to $\cdot OH$.

3) The ROS production ability of energy-sensitive BCNs can be activated or augmented by introducing an additional energy source such as light or ultrasound. For example, thanks to
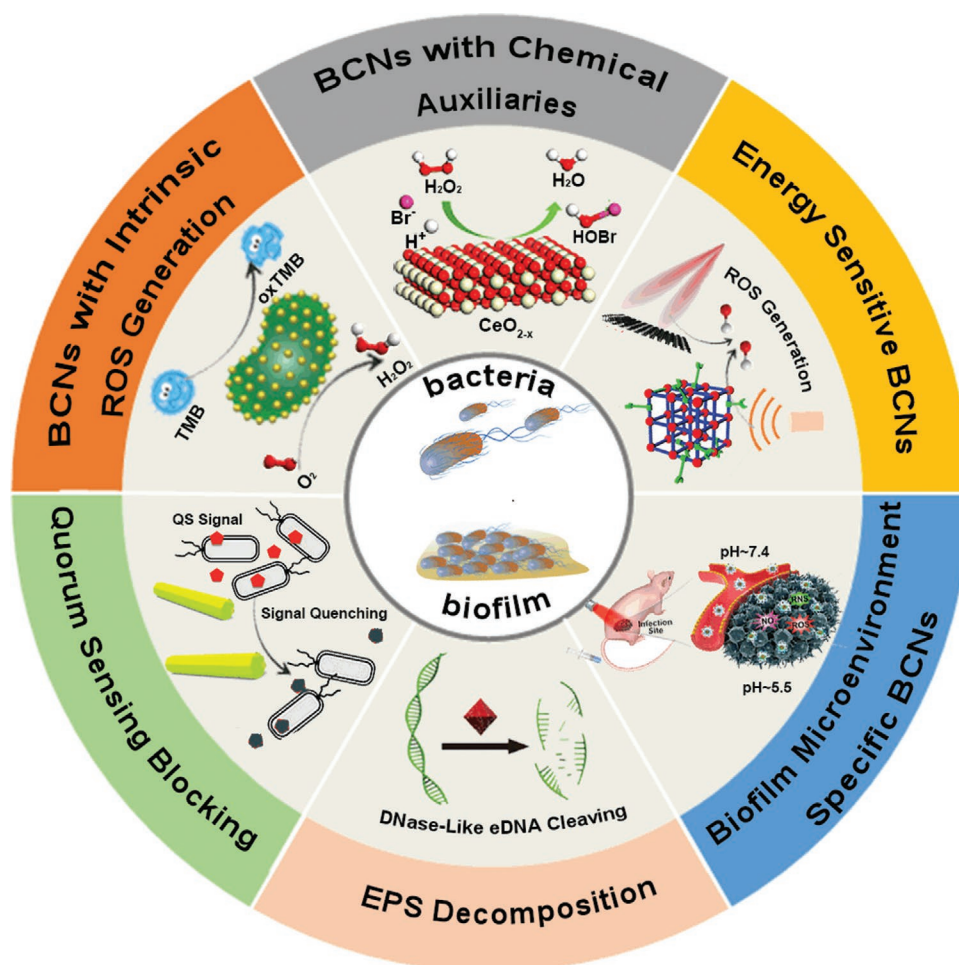
Scheme 1. Classification and antibacterial and antibiofilm mechanisms of BCNs. BCNs with intrinsic ROS generation: Reproduced with permission.[40] Copyright 2015, Wiley-VCH; BCNs with chemical auxiliaries: Reproduced with permission.[41] Copyright 2020, American Chemical Society; energy sensitive BCNs: Reproduced with permission.[42] Copyright 2018, American Chemical Society; EPS decomposition: Reproduced with permission.[43] Copyright 2019, Elsevier Ltd.; biofilm microenvironment-specific BCNs: Reproduced with permission.[44] Copyright 2020, American Chemical Society.

the novel electronic band structure, black phosphorus-based nanocatalysts have been reported as promising candidates in various light-activated dynamic therapies.[54,55] Specifically, they can actively catalyze the generation of $^1O_2$ or •OH upon the introduction of visible light or ultraviolet light, respectively.[42,56] This kind of energy conversion-triggered synergetic modality will not only present a more accurate and controllable therapeutic process but also minimize adverse risks such as the bacterial resistance that can result from relying upon a single bactericidal modality.

4) HPO-mimetic nanocatalysts are reported to block quorum sensing (QS), a cooperative bacterial behavior that affects gene regulation and relies on signal molecules called autoinducers. HPO-mimetic nanocatalysts that can quench autoinducers like N-acyl homoserine lactones have been demonstrated to successfully inhibit biofilm formation.[27]

5) eDNA is regarded to play a major role in maintaining biofilm integrity.[24,57] Hydrolytic BCNs can function as a deoxyribonuclease (DNase), thus cleaving eDNA. DNase-mimetic nanocatalysts are reported to cleave eDNA to disperse and eradicate the formed biofilms.[58]

6) Inspired by tumor microenvironment targeted nanotherapeutics, the biofilm microenvironment (BME) has attracted extensive research interest in recent years.[44,59–63] The salient features of the BME are negative charge, low pH as a result of hypoxia, and high concentration of reductive glutathione (GSH).[60,62,64] Recently designed BCNs with highly pH-dependent or GSH-dependent catalytic activities take advantage of these characteristics to employ BME as coadjutant for highly efficient biofilm eradication.

2.2. Classification of BCNs with Catalytic ROS Production Activities

### 2.2.1. BCNs for Self-Catalytic ROS Production

As we mentioned in the introduction, natural enzymes face a series of challenges in practical production and use. Therefore, researchers have shifted their attention to designing antimicrobial agents with intrinsic bactericidal modalities. For example, metal and metal oxide nanocomposites,

**ADVANCED
SCIENCE NEWS**
www.advancedsciencenews.com

**ADVANCED
MATERIALS**
www.advmat.de

polyquaternium, and carbon-based nanomaterials have been demonstrated to have a strong bactericidal effect via inducing bacterial membrane damage or the accumulation of ROS. However, these antimicrobials' toxicity far exceeds human cellular tolerance, which limits their future clinical application. To address this dilemma, researchers have begun developing BCNs, which could open a new pathway for more sustainable, cost-efficient, and safe antibacterial therapeutics.

Many noble metal-based nanoparticles (NMNPs), such as gold, platinum, and palladium, have been reported as enzyme mimics. It is worth noting that their crystal facets determine the unique catalytic activities of NMNPs, and variations in this feature exhibit significantly different antimicrobial activities. For instance, gold nanoparticles (AuNPs) with different crystal facets have been discovered to exhibit GOx-, POD-, superoxide dismutase-, and catalase (CAT)-mimetic activities. Tao and colleagues synthesized mesoporous silica-supported AuNPs with intrinsic oxidase-mimetic activity (**Figure 1**A,B),[40] which can catalyze oxygen to generate ROS like H_2O_2, single oxygen ($^1O_2$), and superoxide anions ($\bullet O_2^-$) spontaneously under mild conditions. By virtue of this ability, the mesoporous silica-supported AuNPs exhibited robust bactericidal efficacy against *Escherichia coli* and *Staphylococcus aureus* (Figure 1C).

Palladium nanoparticles, another type of NMNP, have recently shown oxidase-mimetic properties. This mechanism was systematically studied via density functional theory (DFT) (Figure 1D),[65] verifying that the oxygen binding and dissociation energy determine the rate of the oxidase-mimicking process of Pd(100) nanoparticles. A morphological study indicated that the bacterial cells take on irregular shapes with wrinkle-like surfaces after treatment with Pd(100) (Figure 1E), indicating the high oxidative stress imposed by oxidase-mimetic Pd(100). Other oxidase nanomimics, like Pt/Ag nanoalloys and silver-graphene quantum dot nanohybrids, also show bactericidal activities.[66,67]

Recently, the Cu_2WS_4 nanocrystals (CWS NCs) were reported to exhibit both oxidase-like and POD-like activities, first binding onto the bacterial outer membrane and then catalyzing nearby oxygen in situ to highly toxic $\bullet OH$ via cascade reaction (Figure 1F).[68] Further experiments demonstrated that CWS NCs at the concentration of 2 µg mL^{-1} can achieve ultra-robust (>99.999%) inactivation of both *E. coli* and *S. aureus*, outperforming the traditional antimicrobials like vancomycin and silver nanoparticles. This work brings not only fresh insights into catalytic bacterial therapy but also suggests new directions for antibiotic development.
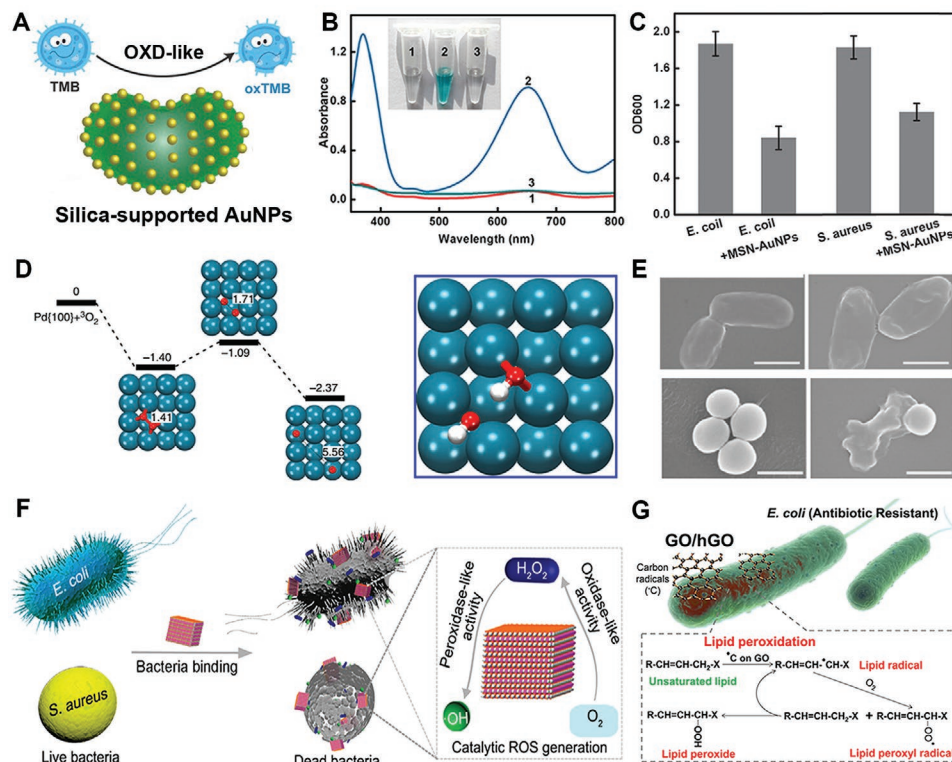

Figure 1. A) Schematic representation of the oxidase-mimetic activities of silica-supported AuNPs (designated as MSN-AuNPs). B) The oxidase-mimetic activity of MSN-AuNPs in different solutions: 1) 3,3′,5,5′-tetramethylbenzidine (TMB) only, 2) TMB with MSN-AuNPs, and 3) TMB with MSN. C) UV–vis absorbance at 600 nm for *E. coli* and *S. aureus* dispersion after treatment with MSN-AuNPs. D) Reaction energies of O_2 on the surface of Pd facet (left) and the lowest energy binding structures for the two hydroxyl radicals on the surface of Pd (111) facet (right). E) SEM images reveal the morphologies of *E. coli* and *S. aureus* before and after Pd (111) treatment. F) Cu_2WS_4 shows bactericidal ability through bacteria surface binding and localized ROS generation via the oxidase-to-POD cascade enzymatic catalysis process. G) Schematic showing the bactericidal mechanism of GO via lipid peroxidation. A–C) Reproduced with permission.[40] Copyright 2014, Wiley-VCH. D,E) Reproduced with permission.[65] Copyright 2018, Springer Nature. F) Reproduced with permission.[68] Copyright 2019, American Chemical Society. G) Reproduced with permission.[69] Copyright 2016, American Chemical Society.

Furthermore, and in contrast to such oxidase-mimicking and POD-mimicking mechanisms, hydrated graphene oxide (hGO) shows significant bactericidal performance toward an antibiotic-resistant *E. coli* strain through catalyzing lipid peroxidation. A mechanistic study showed that the carbon radicals (•C) on the hGO matrix were able to catalyze unsaturated lipid to produce lipid radicals, which then caused lipid peroxidation and membrane damage of the antibiotic-resistant *E. coli* strain (Figure 1E).[69] The development of BCNs with inherently non-invasive bacterial inhibition will open a new pathway for bacterial infection prevention.

2.2.2. Enzyme-Hybrid BCNs for ROS Production

To achieve enzymatic nanoplatforms, the most straightforward methodology is directly doping natural enzymes to obtain enzyme-nanocatalyst hybrids. The large-surface-area matrix of nanomaterials serves as an excellent stabilizer and a protector for natural enzymes within them.[70,71] One representative example is an enzyme that is doped within a metal-organic framework (MOF) scaffold. Zhao and coworkers fabricated a glucose-sensing BCN by loading GOx into an iron-based MOF. This BCN first catalyzes glucose to generate H_2O_2, and then the H_2O_2 is further catalyzed by iron components within the MOF matrix, leading to the oxidation of POD substrate 3,3,5,5-tetramethylbenzidine (TMB) (**Figure 2**A).[72] It is also possible to encapsulate other natural enzymes, or even multiple enzymes, within an MOF. For example, Zhang and colleagues fabricated neutrophil-mimetic nanocatalysts by loading GOx and chloroperoxidase in zeolitic imidazolate framework (ZIF)-8 and then performing a surface modification process via neutrophil membrane coating (Figure 2B–E).[73] In this system, the nanocatalyst's core was able to generate hypochloride via a cascade
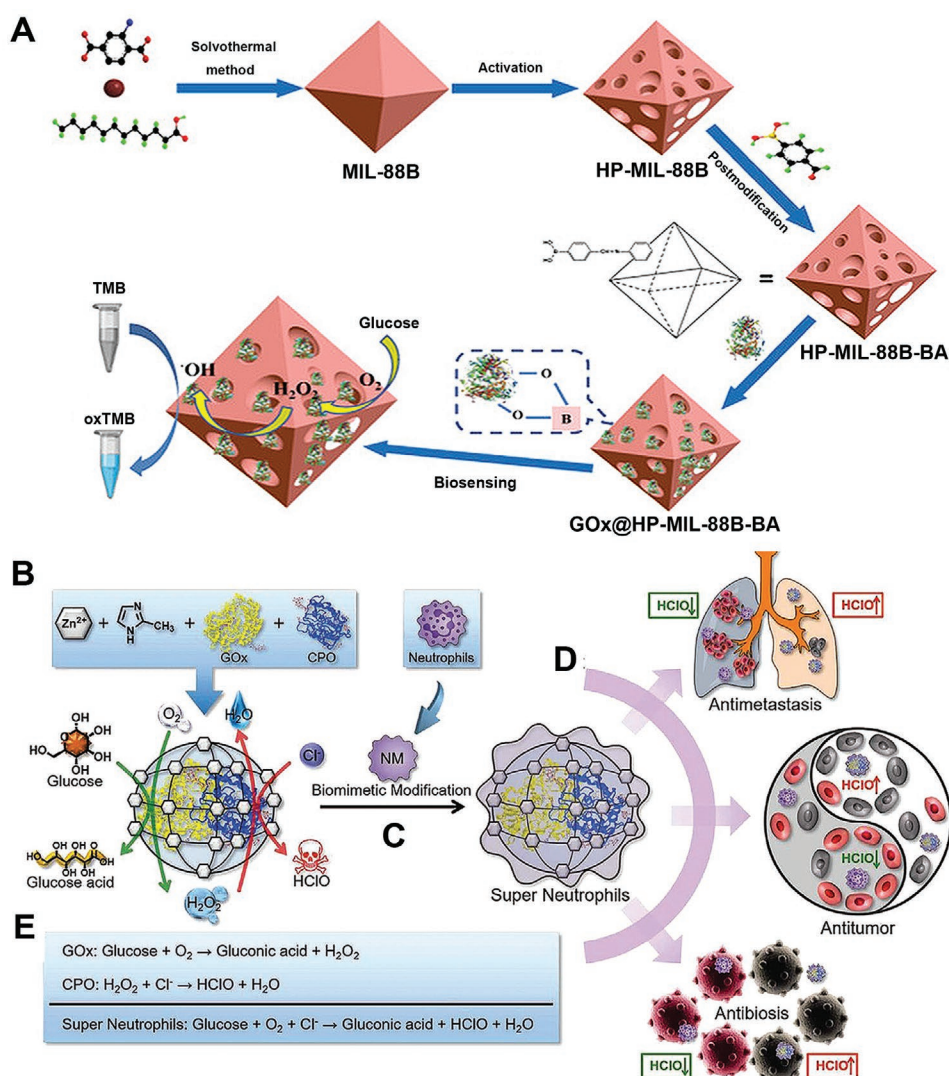
Figure 2. A) The fabrication of GOx-immobilized iron-based BCN for glucose detection. B,C) The synthetic and cascade catalytic processes of hybridized BCNs. D) Wide-ranging applications of biomimetic nanocatalysts with robust HClO generation property. E) The biomimetic nanocatalysts trigger the cascade catalytic reaction mechanism. A) Reproduced with permission.[72] Copyright 2020, American Chemical Society. B–E) Reproduced with permission.[73] Copyright 2019, Wiley-VCH.

catalytic reaction, and the neutrophil membrane shell endowed it with inflammation-specific recognition. Biomimetic nanocatalysts are reported to generate a much higher hypochloride concentration for bacterial disinfection than the natural neutrophils themselves. Apart from MOF-based enzyme-hybridized nanocatalysts, researchers have embedded natural enzymes into numerous nanomaterials, such as mesoporous silica,[5] manganese-based nanostructures,[74,75] nanovesicles,[76] and porous nanocarbons,[75] to achieve high enzymatic activity.

2.3. Chemo-Assisted ROS Production for Bacterial Therapeutics

2.3.1. H_2O_2-Assisted BCNs

As the most commonly used and prevalent ROS, H_2O_2 is considered a primary disinfection reagent for wounds and medical devices in the long term. Due to its high oxidative stress, it disrupts essential biomolecules like lipids, enzymes, and DNA, thus interfering with bacteria's propagation and metabolism. However, this oxidation process is relatively inefficient. Therefore, to achieve desirable disinfection effects, a high dosage of H_2O_2 (up to 1 M) is required, far exceeding the tolerance of healthy tissue nearby and even interfering with wound recovery. Recent research has explored using Fenton-based catalysts like Fe_3O_4 to catalyze H_2O_2 to form more potent ROSs such as $\bullet OH$ and $\bullet O_2^-$, thus potentiating the bactericidal efficacy of H_2O_2 without extra energy input. However, concerns about low catalytic efficiency, as well as intolerable cellular toxicity caused by massive metal ion leakage, press the case for researching BCNs with high efficiency and biosafety.

Researchers have developed various strategies to further improve BCNs' catalytic efficiency, like decreasing their size, alloying, enlarging their specific surface area, or synthesizing nanocrystals with high-index facets. For instance, hollow Pt-based nanocatalysts have been created via chemical deposit and etching (**Figure 3**A–C).[77] The obtained hollow nanocatalysts have been demonstrated to exhibit outstanding POD-like catalytic performance (Figure 3D,E), which can be attributed to the more high-index-facet Pt exposure nanocrystals that serve as active centers. Benefiting from their efficient catalytic performance, the hollow Pt-based nanocatalysts were able to kill *S. aureus* and *E. coli* with a bactericidal ratio of 71.9% under the assistance of only 10 μM H_2O_2. Furthermore, animal experiments revealed that this Pt BCN, under the assistance of a low concentration of H_2O_2, can achieve satisfying wound disinfection outcomes (Figure 3F).

Although noble metal-based BCNs exhibited favorable catalytic stability and activities, their high price and the low utilization efficiency of metal atoms pushed researchers to develop more cost-effective BCNs. Recently, due to their unsurpassed atomic utilization and highly efficient catalytic performance, single-atom nanocatalysts are a burgeoning area of focus of the antibacterial field. More importantly, the single-atom nanocatalysts are architecturally similar to natural enzymes, in that both feature catalytic centers. This structural similarity offers a theoretical basis for the high efficiency of their catalytic performance. Liu and colleagues fabricated a mesoporous ZIF-8 carbon-based BCN containing a single-atomic-zinc central

porphyrin-mimicking structure (PMCS) with a strong POD-mimetic property (Figure 3G).[78] The unsaturated $Zn-N_4$ sites were demonstrated using high-angle annular dark-field scanning transmission electron microscopy (HAADF-STEM) (Figure 3H). The electron spin resonance (ESR) measurement confirmed the high $\bullet OH$ generation after the H_2O_2 was catalyzed by PMCS. Moreover, the catalytic mechanism was studied in detail through DFT calculations (Figure 3I). The catalytic reaction started with the H_2O_2 absorption in the $Zn-N_4$ sites, followed by the dissociation of $H_2O_2^*$ to form two OH^* intermediates via a homolytic path. Afterward, one OH^* intermediate was released and became $\bullet OH$, promoting the catalytic bactericidal process. Moreover, the antibacterial performance is examined both in vitro and in vivo. The *in-vitro* antibacterial data proved that the PMCS showed an extraordinary bactericidal ratio of 99.9% against planktonic *Pseudomonas aeruginosa* (Figure 3J). The in vivo mouse wound healing model provided strong evidence for robust and safe bacterial disinfection via the H_2O_2 catalytic process. This work serves as a paradigm for using single-atom-based nanomaterials for biocatalytic bacterial-related wound disinfection via the POD-mimicking pathway.

Apart from the aforementioned POD-mimetic BCNs, vanadium pentoxide (V_2O_5) nanomaterials showing HPO-mimetic properties have been shown to function as biocatalytic bactericidal nanoagents with the assistance of bromide ions (Br^-) and H_2O_2 via the bromination process. The catalytic mechanism of V_2O_5 nanowires is illustrated in **Figure 4**A.[51] The H_2O_2 first conducts a nucleophilic attack on the surfaces of the V_2O_5 nanowires to form the peroxo complex intermediate. Afterward, Br^- attacks the δ^+ oxygen, leading to the production of HBrO. More importantly, HBrO further reacts with H_2O_2 to generate $^1O_2$ over a long period (Figure 4B), strengthening the bactericidal efficacy. As a result, V_2O_5 nanowires exhibited significant bactericidal performance, with a ratio of 78% against *E. coli* and 96% against *S. aureus* under Br^- and H_2O_2. Unlike the Fenton-catalytic bacterial therapeutics that rely heavily on an acidic environment, this work creates a possible approach for biocatalytic bacterial disinfection in mild alkaline environments like those relevant to ship antifouling coating and seawater sterilization. Similarly, CeO_{2-x} nanorods were also proved to enable morphology-dependent HPO-mimetic properties, which sharply reduced bacterial survival rates after only 5s of coincubation (Figure 4C,D).[41] It is worth noting that as compared to vanadium-based nanocatalysts, cerium-based nanocatalysts show much higher biocompatibility, suggesting new possibilities for clinical antibacterial treatment.

2.3.2. Glucose-Assisted Cascade Enzymatic Reactions

Another exciting trend is the equipment of GOx with POD-mimetic BCNs to enable the cascade enzymatic reaction. In this system, GOx persistently generates abundant gluconic acid and H_2O_2 in situ from glucose, thus avoiding the damage of externally adding non-localized excess H_2O_2. For example, GOx was embedded into POD-mimetic hemoglobin reactors (designated as GOx-Hb) to catalyze a cascade reaction of glucose oxidation and Fenton-like reaction (**Figure 5**A).[79] Significant inhibition was seen in both planktonic MRSA and their biofilm

**ADVANCED
SCIENCE NEWS**

www.advancedsciencenews.com

**ADVANCED
MATERIALS**

www.advmat.de
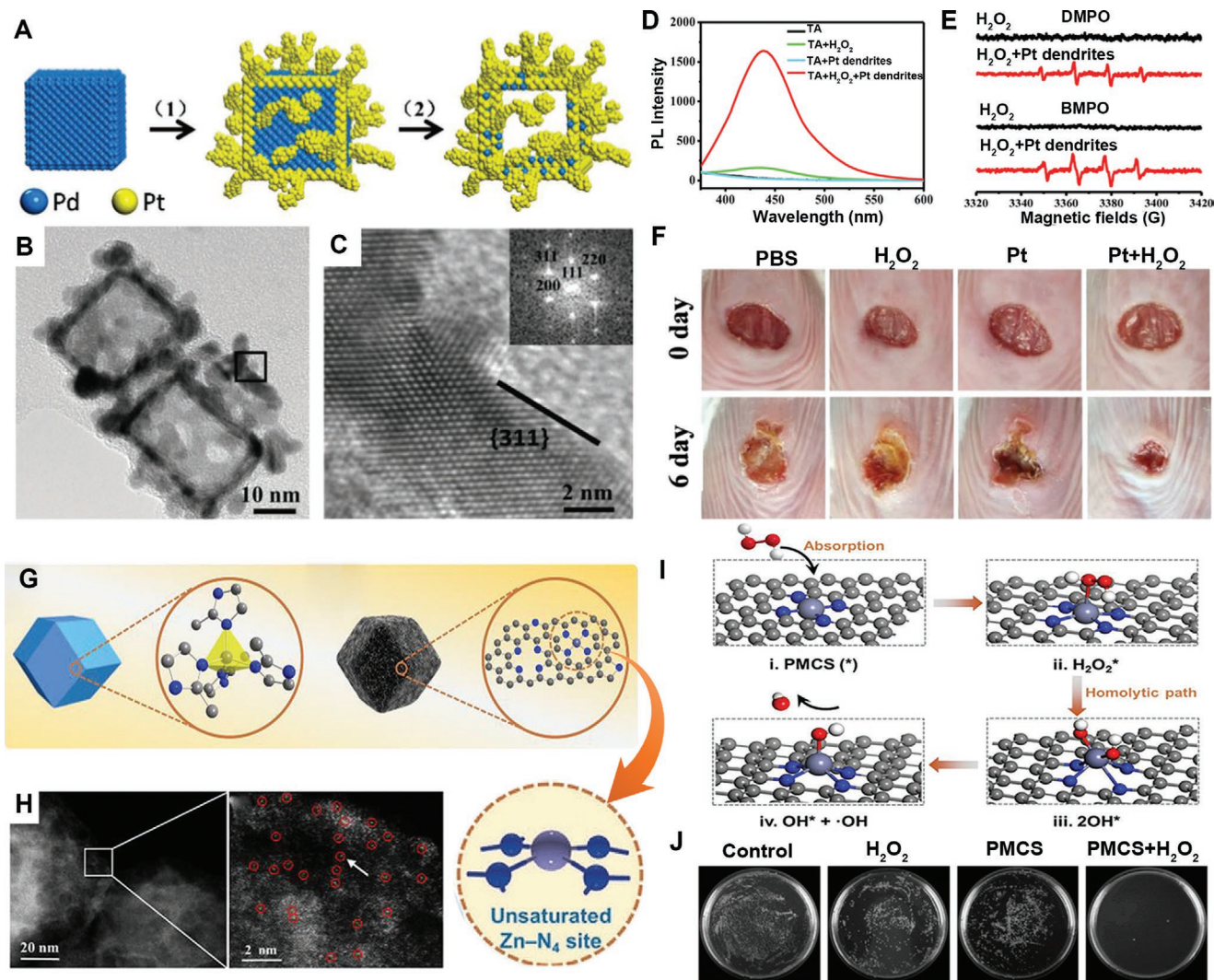
Figure 3. A) Schematic image showing the procedures for the fabrication of platinum hollow nanocatalysts: 1) Pt atoms are first deposited on the Pd nanocubes, then the Pt branches grow and form core-frame nanostructures; 2) Pt hollow nanocatalysts are obtained after $FeBr_3$ etching. B) TEM image of Pt hollow nanocatalysts. C) High-resolution TEM images of Pt hollow nanocatalysts. Scale bar: 2 nm. D) Detection of •OH generated from H_2O_2 after treatment with/without Pt hollow nanocatalysts using fluorescent spectroscopy. E) ESR spectra of samples containing H_2O_2, DMPO, or BMPO, without and with Pt hollow nanocatalysts. F) Representative wound photos of mice during treatment. G) Schematic representation structural model of the precursor ZIF-8 and single-atomic-zinc central porphyrin-like nanocatalysts (designated as PMCS). H) HAADF-STEM images of PMCS, with single zinc atoms marked by circles. I) The DFT calculation for the catalytic mechanism of PMCS. J) Photos of *P. aeruginosa* colonies after different treatments. A–F) Reproduced with permission.[77] Copyright 2018, Wiley-VCH. G–J) Reproduced with permission.[78] Copyright 2019, Wiley-VCH.

after treatment with GOx-Hb (Figure 5B). Recently, Liu and colleagues synthesized a 2D MOF-based BCN (Cu-TCPP(Fe)) that was originated via anchoring GOx onto the surface of a nanosheet to conduct the self-activated catalytic cascade reaction (Figure 5D,E).[53] The 2D BCNs were only able to catalyze TMB to generate oxidized TMB in the presence of 5 mM glucose, verifying their cascade enzymatic ability (Figure 5F).

Moreover, the in situ production of gluconic acid created a localized mildly acidic environment, facilitating the POD-mimetic catalytic process and the generation of toxic •OH radicals (Figure 5G). This cascade enzymatic nanosystem's potent bactericidal efficacy and insignificant biotoxicity were examined by an *in-vivo* wound disinfection model (Figure 5H,I). Similarly, GOx has proven versatile for encapsulation into various

POD-like MOF-originated BCNs for biological applications; examples include NH_2-Fe-MOF,[78] (Fe) MOF-545,[80] ZIF-8,[64,81] FeNi-MOF.[82] These synthesized hybrid BCNs showed outstanding enzymatic cascade performance and remarkable stability over time and in the presence of heat and solvents. Subsequently, AuNPs were proven to be an excellent GOx alternative with much-enhanced stability and lowered cost. Shi and colleagues co-loaded gold and Fe_3O_4 nanoparticles into dendriform silica.[34] In this dual biocatalytic system, in which AuNPs mimic GOx while Fe_3O_4 NPs serve as POD mimetics, the naturally high glucose concentration in the tumor area enables the production of highly toxic •OH in situ, thus achieving excellent therapeutic outcomes. Although this work was directed toward tumor therapy, it is expected that AuNP-loaded nanocatalysts
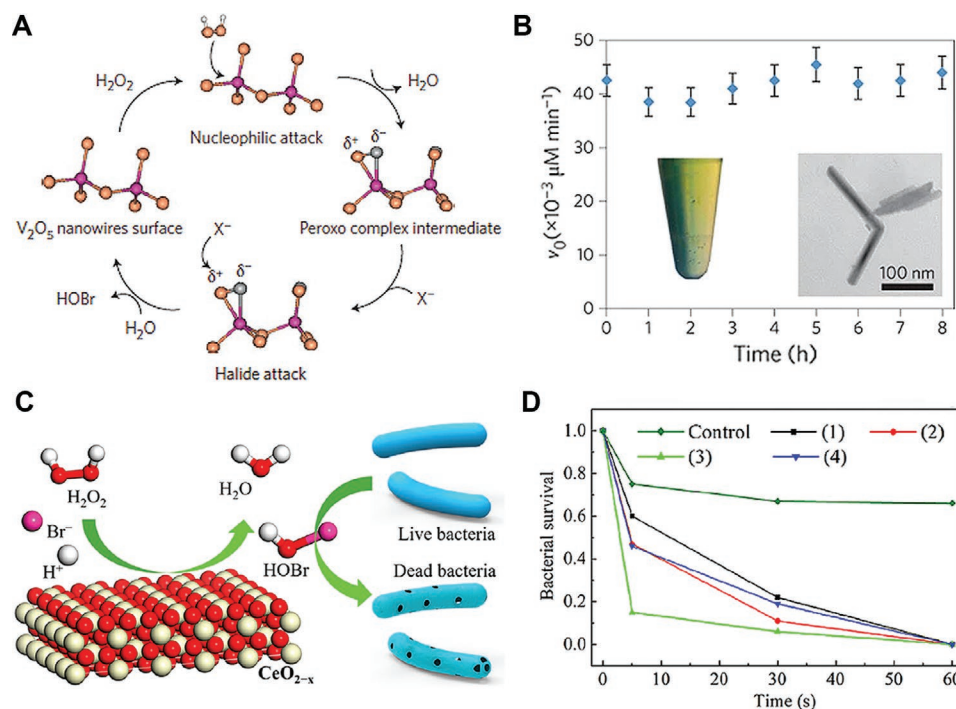
Figure 4. A) Biocatalytic bromination bactericidal mechanism of V_2O_5 nanowires. B) Visible and stable singlet oxygen generation from the V_2O_5 nanowires over a long period. C) Schematic showing that the CeO_{2-x} nanorods could function like HPO and kill bacteria under the assistance of Br^- and H_2O_2. D) Bacterial viability in the solution after treatment by CeO_{2-x} nanorods with aspect ratios: R of 1) ≈13, 2) ≈8, 3) ≈6, and 4) nanopolyhedra in the presence of ammonium bromide and H_2O_2. A,B) Reproduced with permission.[51] Copyright 2012, Springer Nature. C,D) Reproduced with permission.[41] Copyright 2020, American Chemical Society.

with cascade enzymatic capability may also be used for bacterial treatment in the future. These glucose-assisted cascade enzymatic strategies might not only create a novel pathway for antibacterial treatments via self-activated cascade catalytic BCNs, but also enable deep biofilm-related infection therapies.

## 2.4. Energy Conversion Triggered ROS Production for Bacterial Therapeutics

Compared to the endogenously activated chemo-catalytic therapies, the exogenous energy-triggered synergetic modality presents higher bactericidal efficiency and greater flexibility than the local catalytic bacterial treatment. Meanwhile, it minimizes adverse risks like bacterial resistance that can result from a single bactericidal modality. A typical example is photodynamic (PDT) augmented chemotherapy, which combines photosensitive BCNs with traditional chemo-antibacterial agents like chitosan,[42,83] metal ions,[84] antibacterial peptide,[85] and so on. Owing to its intrinsic nature as a photosensitizer, black phosphorus (BP) can act as a ROS generator, thus augmenting composites' bactericidal activities. Mao and colleagues constructed BP nanosheets and incorporated them into chitosan hydrogels (designated as CS-BP) to achieve favorable visible-light-activated bacterial photodynamic disinfection and accelerated wound healing (**Figure 6**A,B,C).[42] Pristine CS hydrogel exhibited endogenic but limited antibacterial activity due to its positive charges. Once BP was embedded, the resultant CS-BP could be used for visible-light-activated PDT (Figure 6D), which

significantly augmented the ablation of *S. aureus* and *E. coli* (Figure 6E,F,G).

Although the above work used photosensitive BCNs to achieve effective sterilization and accelerate wound healing, this nonspecific ROS would still inevitably cause damage to a large number of surrounding cells and tissues. Qu and colleagues constructed a bacterial targeting synergetic biocatalytic PDT nanosystem that is made by coordination of 5,10,15,20-tetrakis(4-methoxycarbonylphenyl)porphyrin (TCPP) and zirconium for on-demand bacterial treatment (Figure 6H).[86] Due to the abundant carboxylic groups and the large specific area, the toxic silver ions were stabilized and loaded into the porous MOF matrix. Afterward, a layer of hyaluronic acid was coated onto the MOF matrix to serve as a shield to prevent the silver ions from leaking and help ensure favorable biocompatibility under physiological or nontargeted bacterial environments. Upon arrival in the targeted bacterial environment containing hyaluronidase, the shield hyaluronic acid layer will be digested. The now-exposed MOF, decorated with positively charged silver ions, can then bind to the bacterial surface via electrostatic interaction and achieve zero-distance poisoning. Meanwhile, the photoresponsive MOF matrix can produce singlet oxygen under visible light, promoting bactericidal efficiency via PDT. This work combines bacterial secreta-responsiveness and electrostatic interaction to endow the BCN with a bacterial targeting effect. However, it should be noted that mammalian cells can also digest hyaluronic acid, which may cause silver ion leakage and potential toxicity.

Interestingly, photosensitive BCNs are also explored in fabricating filtration materials for efficient light-catalyzed air
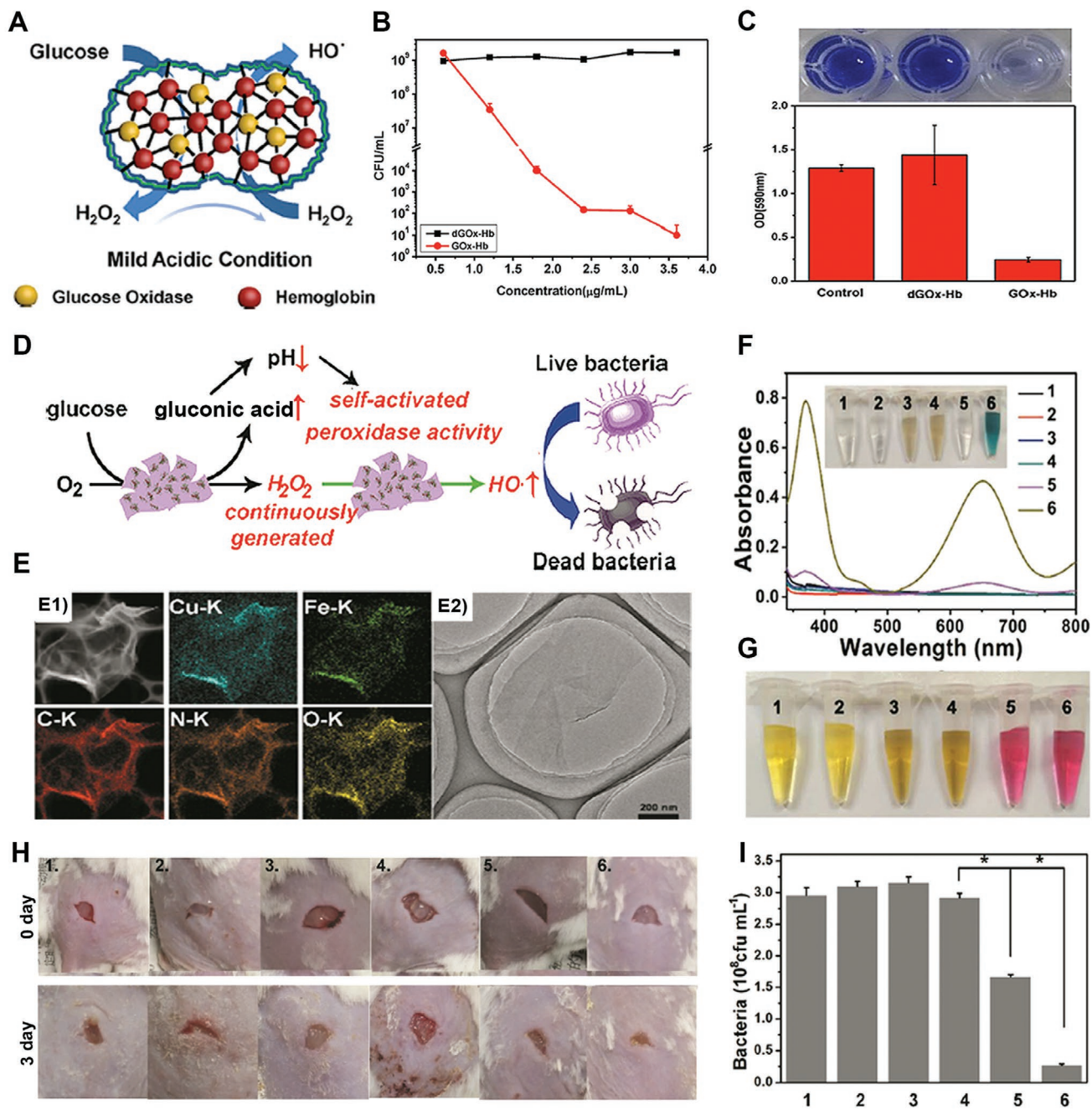
Figure 5. A) Schematic illustration of the nanoreactor cooperation of GOx and hemoglobin (GOx-Hb) in catalyzing glucose to generate •OH under a mildly acidic environment via enzymatic cascade reaction. B) Plate counting results of MRSA treated by GOx-Hb or denatured GOx-Hb (dGOx-Hb). C) Photos of crystal violet stained biofilms after different treatments dissolved by acetic acid and corresponding UV–vis absorbance at 590 nm. D) The self-activated cascade antibacterial process of the 2D MOF/GOx hybrid BCN. E) Darkfield TEM images of 2D MOF-originated BCNs and the element mapping of containing elements (E1), and the representative TEM image of 2D MOF BCNs (E2). UV–vis absorbance spectra and photographs of different reaction solutions containing F) TMB or G) methyl red after a 4-hour-incubation in 0.5 mM of PBS. 1) PBS only; 2) glucose only; 3) glucose and 2D MOF-originated nanosheets; 4) 2D MOF/GOx BCNs; 5) glucose and GOx; 6) glucose and 2D MOF/GOx BCNs. H,I) Photos of wounds after different treatments and the corresponding live bacterial colony. Wounds 1–6 were respectively treated with blank band-aid; glucose; glucose and 2D MOF nanosheet band-aid; 2D MOF/GOx-BCN band-aid; glucose and GOx band-aid; and glucose and 2D MOF/GOx-BCN band-aid. A–C) Reproduced with permission.[79] Copyright 2019, American Chemical Society. D–I) Reproduced with permission.[53] Copyright 2019, American Chemical Society.

sterilization. Very recently, researchers proposed using MOFs as filters for photocatalytic bacterial disinfection in air purification and public hygiene (Figure 6I).[87] Specifically, ZIF-8

synthesized by Zn^{2+} and 2-methylimidazole exhibited ultra-robust bactericidal efficacy against *E. coli* (≈10^6-fold viability decrease) with the assistance of 2 h of visible light irradiation.
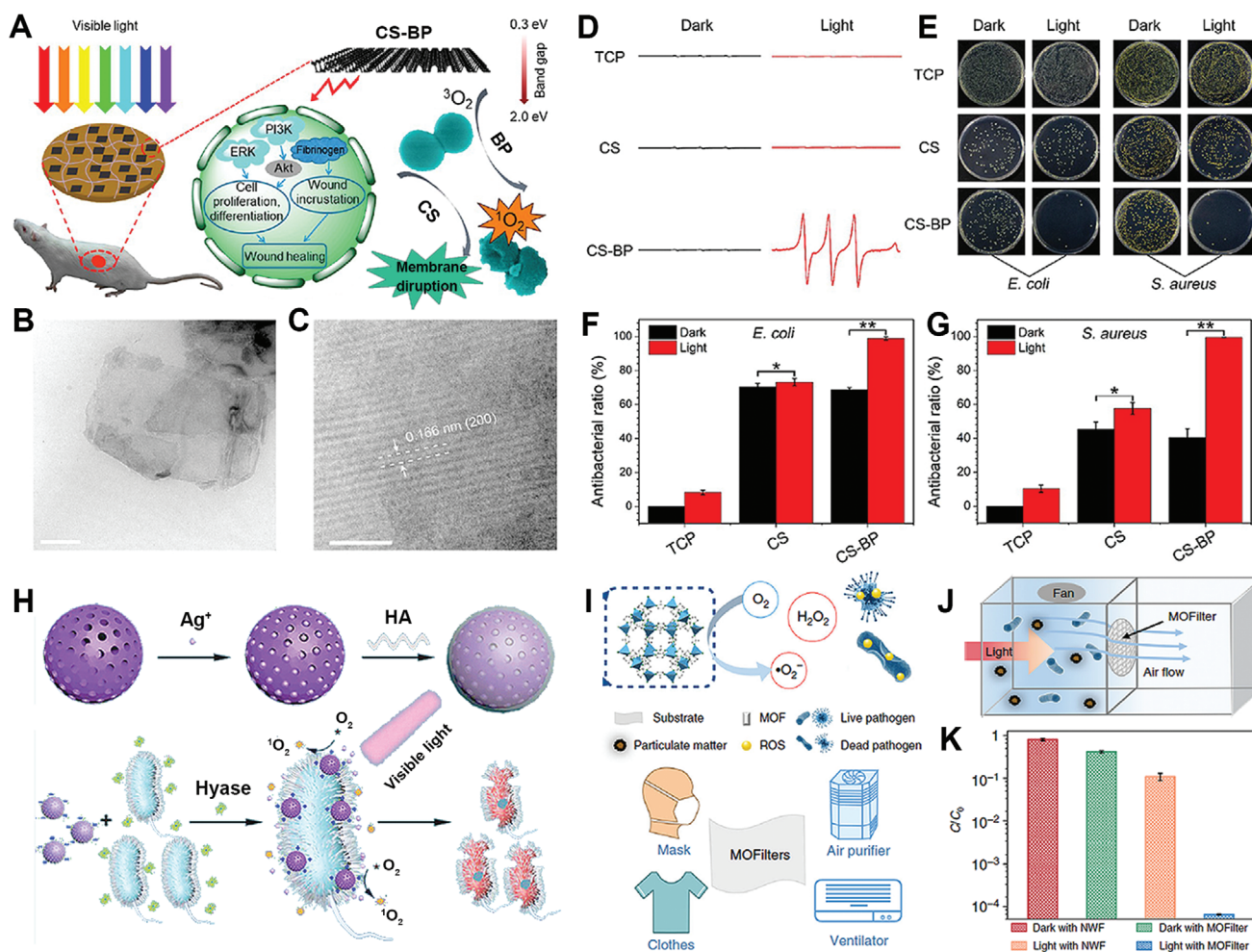
Figure 6. A) Schematic image showing the sterilization process with the assistance of visible light and the cellular promotion property of BP-based hydrogel. B) Morphology of the BPs observed by TEM. Scale bar: 200 nm. C) High-resolution TEM showing the interplanar spacing of 0.186 nm, reflecting the (200) facet. Scale bar: 1 nm. D) ESR spectra were detected from different samples (TCP, CS hydrogel, CS-BP hydrogel) with/without 10-min visible light irradiation in solutions, where 2,2,6,6-tetramethylpiperidine acted as a trapping agent for singlet oxygen. E–G) Bacterial colonies, after treatment with different samples; corresponding quantified antibacterial ratios. H) Scheme of PDT synergetic biocatalytic nanosystem with enhanced bacterial-specific binding and inactivation ability. Schematic illustration of I) the use of MOFs as filters to achieve photocatalytic bacterial disinfection in air purification and public hygiene and J) the air cleaning system model. K) The air disinfection efficiency of ZIF-8 filter and non-woven fabric (NWF) with/without light irradiation. A–G) Reproduced with permission.[42] Copyright 2018, American Chemical Society. H) Reproduced with permission.[86] Copyright 2018, Wiley-VCH. I–K) Reproduced with permission.[87] Copyright 2019, Springer Nature.

Strong evidence has been found that the MOFs' ultra-robust bactericidal efficacy was derived mainly from ROS generation via photocatalysis, while the release of Zn^{2+} from the matrix showed a nonsignificant bacterial viability decrease. Following these results, a mask consisting of ZIF-8 as a filter was assembled to test photocatalytic bacterial disinfection in a practical use situation. Airflow carried particulate matter and *E. coli* bioaerosols to a ZIF-8 filter separating two chambers, and residual bacteria in the second (post-filtration) chamber were quantified (Figure 6J,K). Significantly, the ZIF-8 filter achieved vigorous photocatalytic bacterial disinfection of the air (over 99.99%) within 30 min. This work suggests novel uses of photocatalytic BCNs for air disinfection and personal protection.

In comparison to visible light, the near-infrared (NIR) laser is a better energy source in biocatalytic treatment because it

has high penetration depth, limited tissue damage, and great potential to trigger synergetic effects of PDT and photothermal therapy (PTT).[29,85,88] The synergetic triggering of PDT and PTT by an NIR laser can trade on their distinct but complementary therapeutic modalities to achieve ideal antibacterial performance. For instance, the combined modalities of ROS-triggered oxidative damage toward biomolecules (a chemical modality) and overheating-triggered ablation (a physical mechanism) can be easily implemented in NIR-responsive BCN-based nanosystems.[48,89–91]

Recently, hemoglobin-like carbon-based BCNs with single Fe atoms were reported and designated as SAF NCs; they combine the synergetic effects of PDT and PTT for bacterial disinfection. The single Fe atom within SAF NCs can serve as active sites for producing •OH by catalyzing H_2O_2 under a physiological

**ADVANCED
SCIENCE NEWS**

www.advancedsciencenews.com

**ADVANCED
MATERIALS**

www.advmat.de

concentration (**Figure 7**A).[90] Moreover, upon NIR laser irradiation, the bactericidal efficiency of SAF NCs can be further increased owing to the synergetic modalities of PDT and PTT, leading to bacterial clearance both in vitro and in vivo. Interestingly, as verified by ESR data, the •OH production ability of SAF NCs was strengthened with increasing temperature, demonstrating that the hyperthermia generated during PTT would not only achieve bacterial heat ablation, but more importantly function as a complement to facilitate the PDT procedure (Figure 7B). Owing to these PTT-augmented POD-mimetic modalities, the SAF NCs exhibited remarkable germicidal performance against *E. coli* and *S. aureus* (Figure 7C). This work puts forward a promising strategy for bacterial-related wound disinfection by using carbon-based BCNs with PTT-assisted or PTT-augmented POD-mimetic modalities.

Apart from carbon-based nanomaterials, semiconductors like BP,[42,92] CdTe,[93,94] and molybdenum disulfide (MoS₂)[48,83,91,95] have been investigated extensively for the construction of NIR-augmented synergetic enzymatic therapeutic platforms. Among them, MoS₂ has attracted much attention in biocatalytic antibacterial research because of its excellent biocompatibility and high efficiency of NIR photothermal conversion, and more importantly its inherent POD-mimetic property.[48,91,96] For example, Zhao and colleagues fabricated polyethylene glycol (PEG)-anchored MoS₂ nanoflowers (PEG-MoS₂) as nanosystems for NIR-augmented catalytic antibacterial treatment.[48] The inherent POD-mimetic activity and laser-to-heat conversion of MoS₂ endowed the nanosystems with the PTT-augmented PDT therapeutic effect, and the anchored PEG facilitated the dispersion of the nanosystems. The antibacterial relies on ROS
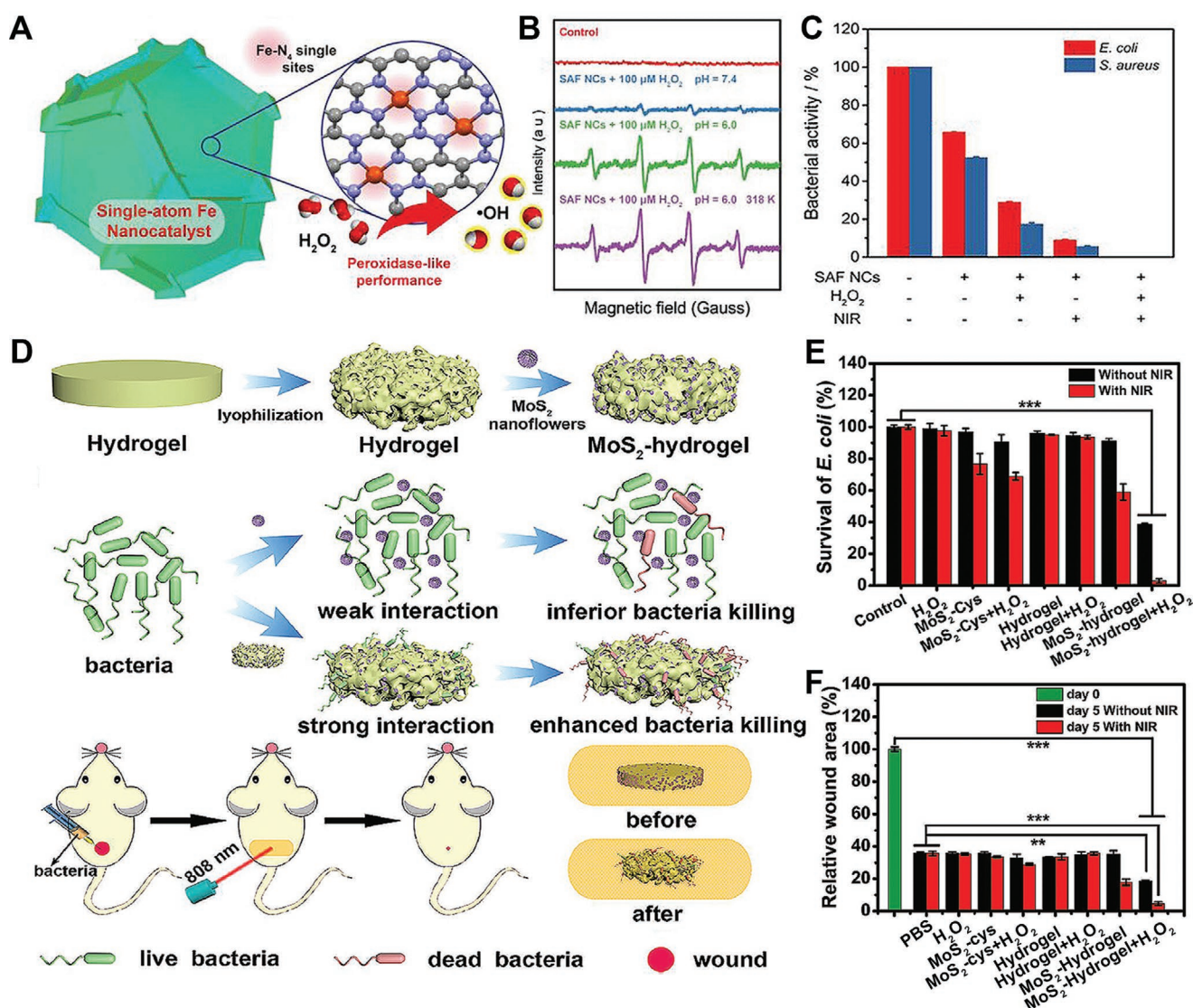

Figure 7. A) Scheme of using BCNs with rich Fe single atomic sites (SAF NCs) to achieve POD-mimetic catalytic performance. B) ESR spectra of solution-dispersed SAF NCs with/without H₂O₂, where BMPO was used as trapping agent. C) Bacterial viability after different treatments. D) Schematic illustration of the synthesis of MoS₂-hydrogel and its application for bacteria clearance and wound disinfection. E) Bacterial viability of *E. coli* after being treated by different samples. F) Wound sizes recorded before and after 5 days' treatment with different samples. A–C) Reproduced with permission.[90] Copyright 2019, Wiley-VCH. D–F) Reproduced with permission.[91] Copyright 2019, Wiley-VCH.

**ADVANCED
SCIENCE NEWS**

www.advancedsciencenews.com

**ADVANCED
MATERIALS**

www.advmat.de

exposure rendering the bacterial membrane vulnerable and penetrable, resulting in higher hyperthermal sensitivity and a shorter duration of the therapeutic procedure. More importantly, the NIR-laser-heated PEG-MoS$_2$ showed intensified GSH oxidation, thus destroying the bacteria's defenses against oxidative stress and further strengthening the bactericidal activity. With its multiple modalities for countering bacterial infection, the PEG-MoS$_2$ was regarded as an emerging candidate for highly efficient bacterial clearance both in vitro and in vivo. This work creatively applied the 2D MoS$_2$ as a POD mimetic to advance antibacterial and wound disinfection research, providing a new possibility for constructing a 2D PTT-augmented PDT catalytic platform for clinical antibacterial therapy.

However, it is worth mentioning that the ultra-short lifetime (<0.2 μs) and limited diffusion range (approximately 20 nm) of ROS severely interfere with the therapeutic effect of BCNs. Besides, after being killed, the bacteria will still accumulate in the infected area and give rise to undesirable inflammation, slowing down the wound healing. To address these issues, Qu et al. embedded MoS$_2$ nanoflowers in a hydrogel, designated as MoS$_2$-hydrogel, for wound dressing. This method not only spontaneously trapped bacteria and killed them under the range of PTT-induced hyperthermia and PDT-generated ROS; it also removed the dead bacteria from the wound, reducing the inflammation reaction and promoting wound healing (Figure 7D).[91] Antibacterial experiments both in vitro

and in vivo provided strong evidence for the robust NIR-augmented bacterial disinfection property of the MoS$_2$-hydrogel (Figure 7E,F). The interaction of 2D nanocatalysts with a 3D hydrogel scaffold represents a novel concept for constructing BCNs that combine spontaneously bacterial trapping, killing, and removal ability for wound treatment without inflammation.

In addition to synergetic ROS-assisted PDT-PTT strategies, nitric oxide (NO)-enhanced PDT-PTT is also a strategy for bacterial treatment.[97,98] NO can significantly interfere with bacterial growth by directly reacting with bacterial DNA and thwarting its recombination.[99–101] Moreover, in the presence of ROS, NO can be transformed into peroxynitrite (ONOO⁻), which has been shown to exhibit bacterial toxicity by exerting high peroxidative stress toward the bacterial membrane.[45,102] Recent studies show that l-arginine can be oxidized via biocatalytic reactions to produce NO in the presence of NO-synthasen (iNOS), NADPH, and ROS (**Figure 8**A).[61,97,103,104] Inspired by this, Cai and coworkers designed cascade BCNs by loading l-arginine and indocyanine green (ICG) into mesoporous polydopamine for bacteria and biofilm treatment. (Figure 8B)[61] The cascade catalytic reaction starts with $^1O_2$ generation by the photosensitizer ICG upon exposure to NIR laser; from there, l-arginine catalyzed NO formation. Subsequently, the NO further reacted with part of $^1O_2$ and became ONOO⁻. This NO-enhanced PDT disrupted the membrane structure of bacteria and thus increased their sensitivity to heat. In this way, robust
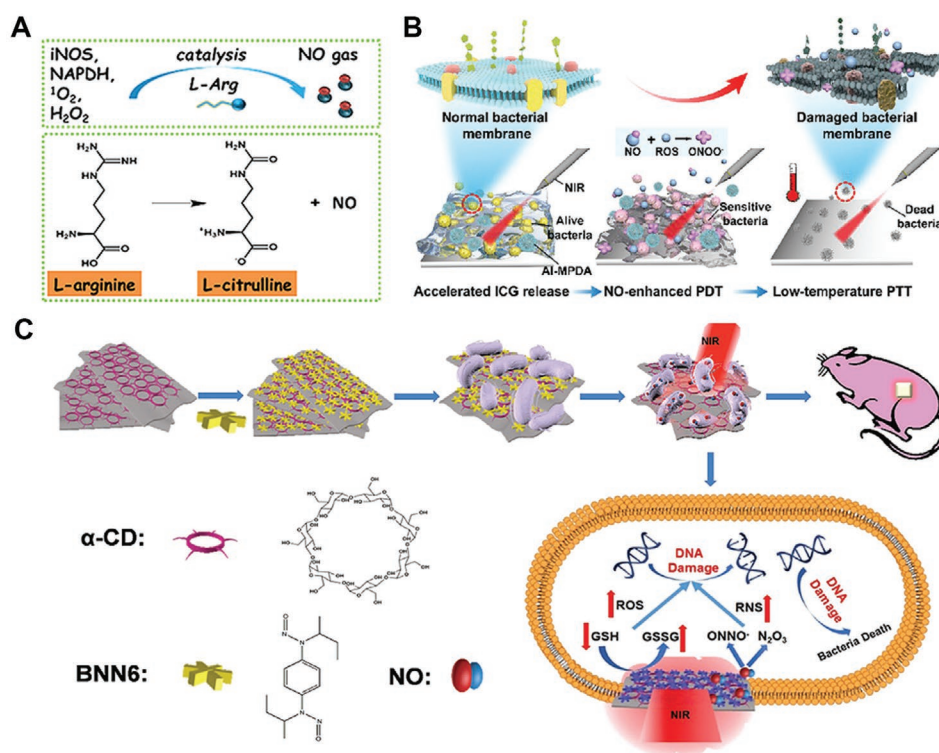

Figure 8. A) Schematic showing NO production from L-arginine (L-Arg). B) Scheme of using an NO-enhanced PDT-PTT strategy to remove established biofilm. In this cascade catalytic nanoplatform, first, ICG and L-Arg produced ROS and NO under NIR laser. ROS was then able to further react with NO to form more toxic RNS. Consequently, the biofilm eradication was successfully realized under moderate PTT treatment, since the NO-enhanced PDT had weakened the bacteria and made them more sensitive to heat. C) Scheme of using 2D MoS$_2$-BNN6 with PTT-enhanced NO production and GSH consumption performance as bactericidal wound disinfection agent. A,B) Reproduced with permission.[61] Copyright 2020, American Chemical Society. C) Reproduced with permission.[95] Copyright 2018, Wiley-VCH.

**ADVANCED
SCIENCE NEWS**

www.advancedsciencenews.com

**ADVANCED
MATERIALS**

www.advmat.de

biofilm eradication were achieved by this nanoplatform under very moderate PTT conditions (≤45 °C), decreasing the potential side effects to the tissue nearby.

NO-enhanced PDT-PTT synergetic effect was also achieved in 2D nanoplatforms. A 2D BCN (designated as MoS_2-BNN6) was fabricated by loading N,N'-di-sec-butyl-N,N'-dinitroso-1,4-phenylenediamin (BNN6) into an α-cyclodextrin (α-CD)-assembled MoS_2 nanosheet. This BCN was designed to achieve NO-enhanced PDT-PTT antibacterial treatment (Figure 8C).[95] In this nanoplatform, the thermoresponsive component BNN6 acted as a controllable donor that produced NO when heated by hyperthermia during NIR-triggered PTT. Through another pathway, the nanoplatforms showed excellent GSH consumption ability, leading to the accumulation of ROS in the bacterial cell. The ROS and reactive nitrogen species (RNS) simultaneously resulted in bacterial death by causing damage to the DNA. By the synergetic effects of PTT and ROS- and RNS-based PDT, the nanoplatforms achieved highly effective bacterial inactivation on short notice. Moreover, as validated in animal experiments, the nanoplatforms also showed a favorable ability to repair wounds and minimize inflammation. Further experiments verified that MoS_2-BNN6 not only effectively killed both *E. coli* with ampicillin-resistance and *Escherichia faecalis* bacteria with heat-resistance, but also achieved significant wound disinfection efficacy. As compared to the traditional ROS-assisted

PDT-PTT nanosystems, these BCNs with NO-enhanced PDT-PTT effect achieved more effective bacterial and biofilm elimination under shorter PTT duration. However, NO-enhanced PDT always relies on the participation of the NO donor, which will not only complicate the synthesis of BCNs but will also affect their stability.

Due to recent progress in sonocatalytic therapy (SCT), the application of ultrasound (US) has emerged as a trend for activating sonosensitive BCNs for deep bacterial infection treatment.[105] Pang and colleagues proposed sonocatalytic bacteria-specific nanosystems for combating multidrug-resistant bacteria. They synthesized these nanocatalysts by co-loading the sonosensitizer purpurin 18 (P18) and maltohexaose-modified cholesterol into 1,2-dioctadecanoylsn-glycero-3-phospho-(1′-racglycerol) (DSPG)-based nanoliposome. Therein, maltohexaose served as a guide to bacterially infected sites; the DSPG-nanoliposomes were then decomposed by bacterial phospholipase and released the P18. Once stimulated by the US, the P18 generated abundant ROS and completed the sonocatalytic bactericidal procedure. Subsequently, in another representative work, Zheng et al. constructed a sonosensitive biocatalytic nanoagent, Pd@Pt-T790, for sonocatalytic treatment of MRSA-induced myositis (**Figure 9**A).[106] In this work, the addition of the sonosensitizer mesotetra(4-carboxyphenyl)porphine (T790) dramatically inhibited the CAT-mimetic ability of Pd@Pt in
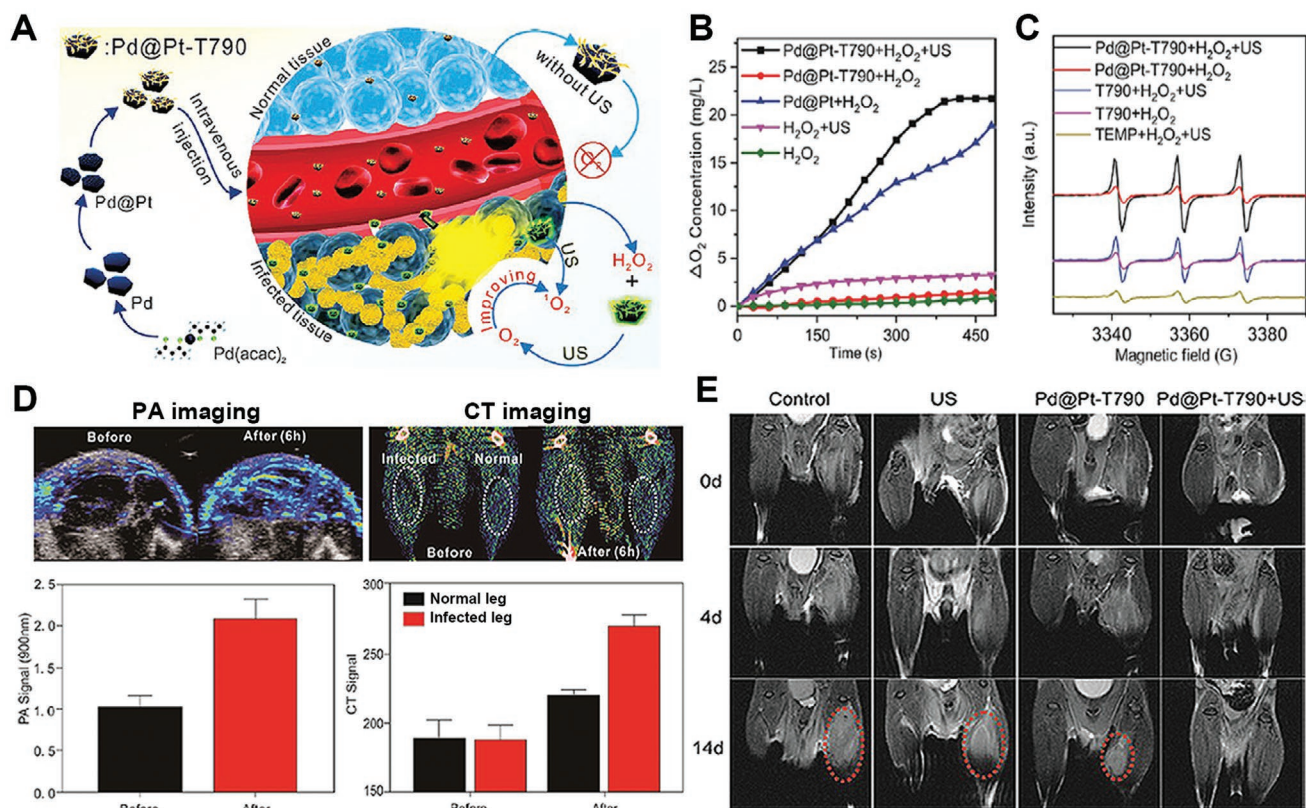
Figure 9. A) Schematic showing the main fabrication procedure of the Pd@Pt-T790 nanoagent and its US-controllable oxygen-rich enhanced SCT against deep bacteria-related inflammation. B) O_2 generation by Pd@Pt-T790 without or with US irradiation. C) ESR spectra of $^1O_2$ in different sample dispersions with/without US treatment (TEMP was used as trapping agent). D) In vivo images of PA (left) and CT (right) and corresponding signals of mice legs before and after 6 h of Pd@Pt-T790 treatment. E) MRI images of infected areas treated with different conditions. Reproduced with permission.[106] Copyright 2020, American Chemical Society.

ADVANCED
SCIENCE NEWS
www.advancedsciencenews.com

ADVANCED
MATERIALS
www.advmat.de

the absence of US. The introduction of US then effectively restored the biocatalytic behavior inherent to Pd@Pt, creating an oxygen-rich environment and thus accelerating ROS generation in the SCT process (Figure 9B,C). Interestingly, these nanocatalysts also functioned as photoacoustic and computed tomography-imaging agents, which could be easily localized and monitored during the therapeutic process (Figure 9D). Moreover, magnetic resonance imaging (MRI) revealed that the MRSA-induced myositis was eradicated under the combined treatment of Pd@Pt-T790 and the US (Figure 9E). Although these works are based on the loaded sonosensitizer for ROS generation under US stimulation, we anticipate that BP or other BCNs with intrinsic sonocatalytic ROS production can also be applied to construct the SCT platform for antibacterial therapy in the short run.[107,108]

2.5. Designing BCNs for Biofilms' Eradication

2.5.1. Blocking QS in Biofilms

Quorum sensing (QS) is an intercellular communication method that empowers planktonic bacteria to recognize their group, which is regarded as the first step for biofilm formation.[109] Specifically, bacteria conduct QS via sensing the signal molecules, that is, autoinducers like N-acyl homoserine lactones (AHLs).[110] Therefore, methods that use autoinducers' competitors or quenchers have been put forward as a novel pathway for biofilm inhibition. Illuminated by the bactericidal mechanism of algae using HPOs to produce hypohalous acid in the marine environment, the HPO-mimetic BCNs that we mentioned in Section 2.3.1 also show great biofilm inhibition potential, since the catalysate hypohalous acid can oxidize and quench AHLs (**Figure 10**A,B).[111] Tremel and colleagues discovered that HPO-mimetic CeO_{2-x} nanorods showed the ability to recreate this plot when used as additives for seawater paint, thus achieving robust biofilm prevention performance (Figure 10C). Subsequently, CeO_{2-x} nanorods were also electrospun with polyvinyl alcohol to fabricate nanofibrous mats, which showed catalytic ability to produce HOBr for bacterial disruption of QS.[112] These works represent an entirely new concept for emulating marine organisms' defense mechanism for inhibiting bacterial recognition and biofilm establishment. Besides, another HPO mimetic, V_2O_5 nanowires (NWs), could produce HOBr in the presence of H_2O_2 and Br^-, thus interfering with the QS system of bacteria and preventing bacterial adhesion (Figure 10D).[51] After being soaked in the ocean for 60 days, the samples comprising V_2O_5 did not indicate biofouling (Figure 10E). Although vanadium-based BCNs were reported to be mutagenic, carcinogenic, and teratogenic,[111] their environmental friendliness and robust stability in the presence of heat and solvents[113] mark them as prospective weapons for biofilm prevention in a wide range of environments.

2.5.2. Decomposition of EPS

Once biofilm forms, the EPS functions as a powerful barrier that can physically block the penetration of antimicrobials and negate their bactericidal modality. In terms of structure and composition, eDNA, polysaccharides, and proteins, as significant components of EPS, create a robust but flexible structure to encapsulate and protect bacteria inside.[114] Therefore, EPS should be considered as the first opponent in any effort to eradicate mature biofilm. As a bridge for connecting bacterial cells and the other EPS components, eDNA plays a key role in maintaining biofilm's stability and integrity.[115] Hence, the cleavage of eDNA is a promising strategy for disintegrating biofilms by alienating the EPS components.[58,116] In recent years, some BCNs have been reported to function as a nuclease. For instance, Kuang and co-workers demonstrated that CdTe nanoparticles can function as endonuclease mimetics upon light irradiation.[117] Furthermore, copper-ion-loaded graphene oxide nanosheets were reported to show potential in DNA cleavage.[118] However, their broad application in combating biofilm are limited by the high cytotoxicity of the released metal ions.

Recently, Ce(IV)-based BCNs with high catalytic activities and excellent biocompatibility were reported to mimic DNase to hydrolyze DNA or RNA.[119] Xu et al. systematically studied the DNase-mimicking activity of CeO_2 nanoparticles. They proposed the catalytic mechanism as follows: first, Ce centers combine with the non-bridging oxygen atoms in the phosphate group; afterward, a hydroxide ion bound to the Ce center conducts a nucleophilic attack on the phosphorus atom and triggers the cleavage of DNA. (**Figure 11**A).[120] Also, BCNs with DNase activity have been synthesized by conjunction cerium complexes on AuNPs embedded on Fe_3O_4/ SiO_2 nanoparticles. Anti-biofilm experiments verified that this BCN showed significant inhibition of bacterial colonization, with a ratio of up to 90%. More importantly, even for the 120-hour-aged dense biofilms, the BCN exhibited a robust DNase-mimetic activity, thus leading to the disintegration of biofilms.[58]

Based on this work, more recently Qu and colleagues united two kinds of enzyme mimics for the construction of a BCN that could not only thoroughly eradicate established mature biofilms but also effectively prevent biofilm recurrence. In their work, an Au-loaded iron-based MOF was first synthesized as an intrinsic POD mimic. Afterward, cerium-based complexes were assembled on the MOF-Au, endowing the BCN with DNase-mimetic properties. The nanocatalysts, namely, MOF-Au-Ce, could then combat biofilm with both POD-mimetic and DNase-mimetic modalities (Figure 11B,C).[43] The DNase-mimetic mechanism of the cerium center is more or less the same as in Qu et al.'s previous work (Figure 11D). The agarose gel electrophoresis data demonstrated that MOF-Au-Ce could cleave and even achieve total degradation of both *S. aureus'* small single-strand DNA and its genomic DNA at a concentration of 0.5 mg mL^{-1}. The antibacterial treatment validated that the MOF-Au-Ce itself could only induce biofilm dispersion, while after introducing H_2O_2, MOF-Au-Ce was able to eradicate the majority part of biofilms (Figure 11H). These results proved the concept that BCNs with complementary DNase and POD activities show great potency for biofilm eradication by releasing ROS and causing biofilm dispersion. These DNase-mimetic nanocatalysts provide effective ways of combating established dense biofilm.
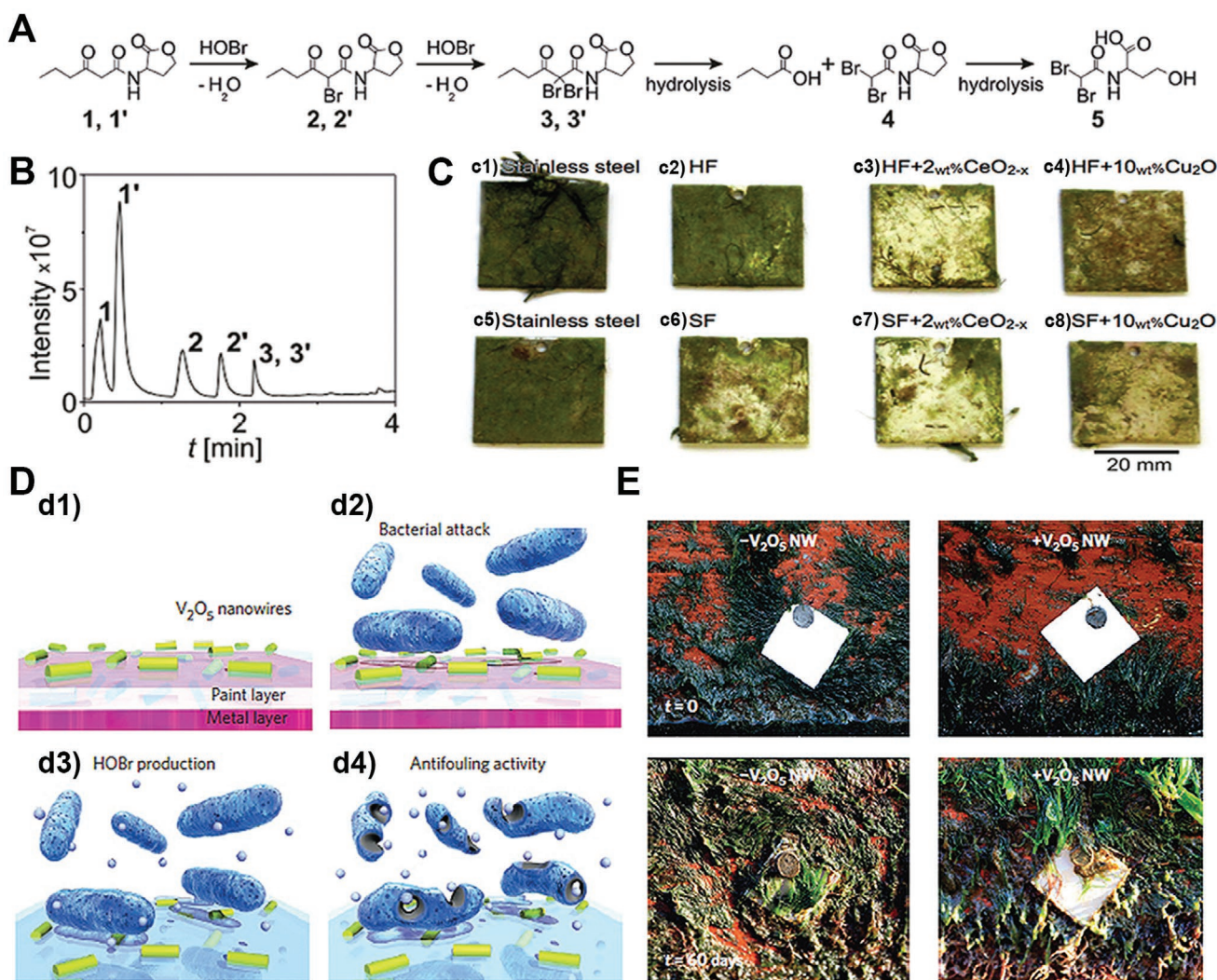
Figure 10. A) The CeO_{2-x} catalyzed quenching of AHL via bromination and hydrolysis reactions. B) Ion chromatography was used to detect the products during the catalytic bromination reaction. C) Photos of samples after a 7.5-week soaking procedure. Samples (c1, c5) were pristine stainless-steel substrates; commercial hard (c2, c3, c4) and soft (c6, c7, c8) antifouling coatings, with (c3, c7) or without (c2, c4, c6, c8) cerium dioxide nanoparticles, were coated to substrates. D) Bacteria colonization inhibition process of V_2O_5 nanowires (NWs). d1) NWs are located on the surface. d2) Bacteria approach the surface. d3) NWs enable hypohalous acid generation. d4) The bacteria's death is caused by highly oxidative hypohalous acid. E) Photos of stainless-steel substrates with/without V_2O_5 NW coating on day 0 and day 60. A–C) Reproduced with permission.[11] Copyright 2017, Wiley-VCH. D,E) Reproduced with permission.[51] Copyright 2012, Springer Nature.

2.5.3. BME-Targeted Strategies

In recent years, the focus of designing anti-biofilm BCNs gradually shifted from nonspecific invasiveness to targeted elimination via recognizing the biofilm microenvironment (BME), which is characterized by hypoxia, acidosis, and highly reductive conditions.[44] Under the hypoxic conditions of BME, it is difficult for general BCNs to achieve the desired performance. For example, oxygen is of vital importance to ROS production in some kinds of BCN-based therapies.[65,66,74,121] However, in the hypoxic BME, the amount of ROS generated will be significantly reduced, thus decreasing therapeutic efficacy. Besides, as in some GOx/BCN hybrid systems, the lack of oxygen weakens the enzymatic activity of GOx and slows down the entire cascade catalytic reaction.[74] Up to now, CAT-mimetic

BCNs like Pt-based nanohybrids,[85,91,121,122] Mn-based MOF NPs,[123] Co_3O_4,[124] MnO_2,[74] MoO_{3-x},[125] IrO_2,[126] and so on, have been validated to generate oxygen in the presence of H_2O_2, which can significantly improve the hypoxic condition and therapeutic efficacy. Even more promisingly, very recently CuO_2 was demonstrated to show both H_2O_2-self-supplying and POD-mimetic properties; it can therefore generate •OH itself and overcome the oxygen dependence of PDT. Although many publications have focused on improving hypoxic conditions in the tumor microenvironment, CAT-mimetic BCNs show great potential for combating biofilm-related deep infections.

Furthermore, the acidic condition of BME (pH 4.5–6.5) due to anaerobic bacterial respiration could be used as a distinct trigger for certain pH-dependent nanocatalysts to achieve biofilm-specific treatment.[127] For instance, based on the Fenton
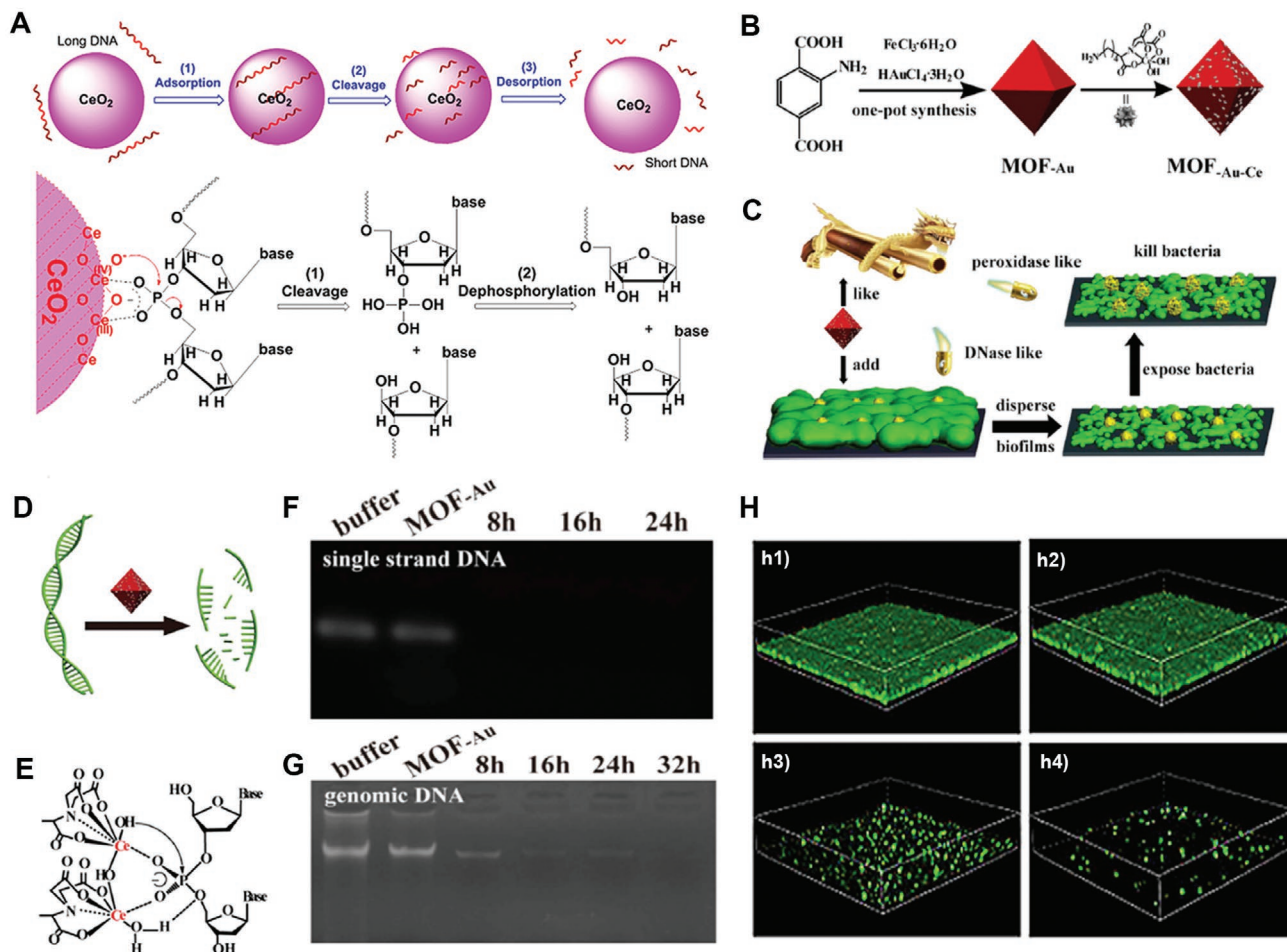
Figure 11. A) Schematic illustration of the DNA cleavage procedure catalyzed by DNase-mimetic CeO_2. Schemes showing B) the fabrication of MOF_{-Au-Ce} and its C) DNase/POD-mimetic modalities for biofilm dispersion and eradication. Schemes of D) DNA cleavage function and E) mechanism of MOF_{-Au-Ce} via nucleophilic attack toward phosphorous atom induced by hydroxide ion bonding on the cerium center. F) Small single-strand DNA and G) genomic DNA of *S. aureus* incubated with 0.5 mg mL^{-1} of samples for different times. Column 1: buffer only; column 2: treated with MOF_{-Au}; remaining columns: treated with MOF_{-Au-Ce} for different incubation times. H) Z-stack images acquired by confocal laser scanning microscopy (CLSM) of 12-hour aged biofilms treated for 12 hours with h1) no additives; h2) H_2O_2; h3) MOF_{-Au-Ce}; h4) MOF_{-Au-Ce} and H_2O_2. The biofilms were labeled with FDA for CLSM. A) Reproduced with permission.[120] Copyright 2019, Royal Society of Chemistry. B–H) Reproduced with permission.[43] Copyright 2019, Elsevier Ltd.

mechanism, iron oxide has demonstrated outstanding POD-mimetic performance under a mildly acidic environment consistent with BME conditions.[128] Koo and coworkers exploited this attribute in successfully using dextran-coated ferrous BCN to eliminate periodontal biofilms.[63] The kinetic determination revealed the catalytic activity of the BCNs was remarkable at a pH of 4.5 but negligible at a pH of 6.5. This distinct pH selectivity endows this BCN with highly BME-specific toxicity but excellent safety toward a healthy oral cavity. This work provided new inspiration for using Fenton-based BCNs for pH-induced biofilm-specific treatment, but it should be noted that the leakage of metal ions might be harmful to healthy tissue nearby. In another representative work, BCNs with BME-specific recognition and imaging were fabricated by loading ruthenium-based catalysts into pH-responsive ligand-conjugated AuNPs (**Figure 12**A).[60] The pH-induced BME-specific recognition was triggered by the charge changing from zwitterionic to cationic

on the surface of BCNs under BME conditions, facilitating the penetration of BCNs into the biofilm. Afterward, the loaded Ru-catalysts catalyzed a non-fluorescent substrate to form a fluorescent product, thus labeling and locating the biofilm area. Very recently, Zhang and colleagues designed a bioresponsive BCN consisting of spiropyran and galactose for selectively locating and eliminating biofilm in situ.[59] In this system, the nanoplatform was able not only to specifically bind to *P. aeruginosa* via galactose-lectin interaction, but also to emit red fluorescence and generate ROS under a mildly acidic BME, thus achieving a smart biofilm-targeting binding-locating-eliminating biocatalytic therapy. These works present novel strategies for efficiently and specifically locating biofilms growing in complicated physiological conditions, creating a new pathway for imaging and eliminating in vivo biofilm-related infections.

The high concentration of reductive GSH in biofilms is another important factor limiting the efficacy of BCNs

ADVANCED
SCIENCE NEWS
www.advancedsciencenews.com

ADVANCED
MATERIALS
www.advmat.de
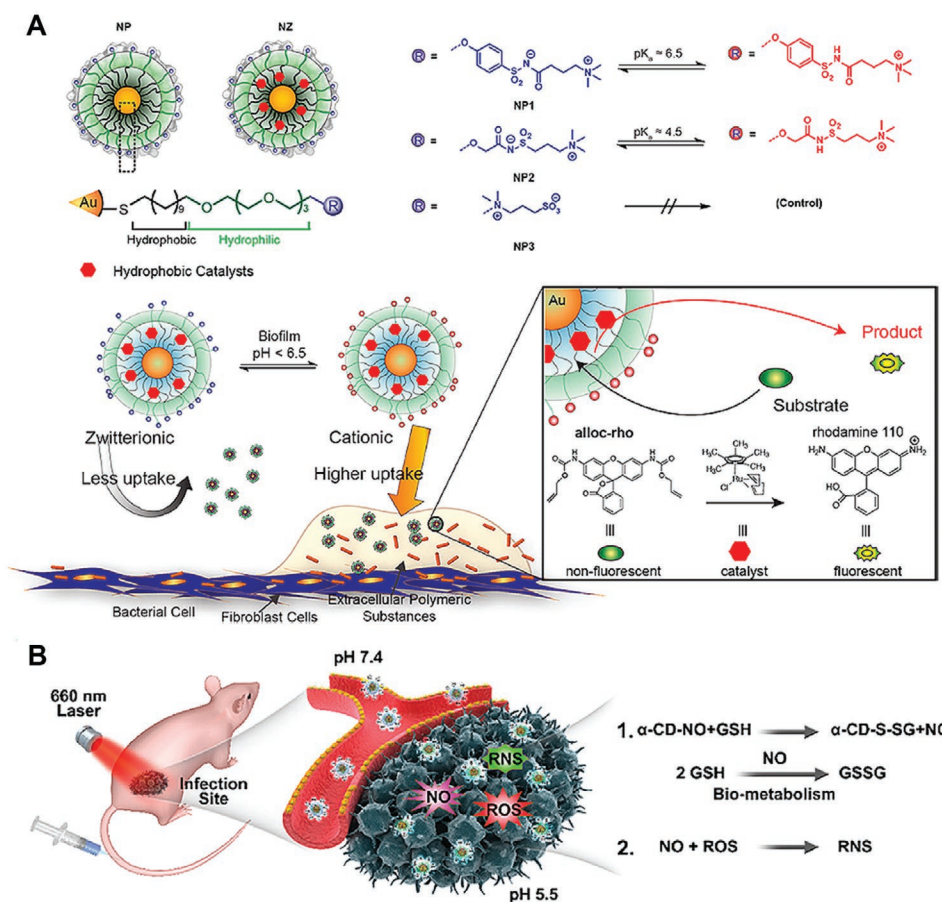
Figure 12. A) Schematic image showing the specific locating of infectious biofilm sites using Au-based nanocatalysts with pH-induced surface charge changing ability. B) Schematics showing the biofilm-related infection treated by GSH-responsive nanocatalysts via NO-enhanced PDT. A) Reproduced with permission.[60] Copyright 2018, American Chemical Society. B) Reproduced with permission.[44] Copyright 2020, American Chemical Society.

because it can gratuitously consume the ROS generated by BCNs.[129] Therefore, Ji and colleagues reported the employment of a GSH scavenger as a coadjutant for laser-assisted biocatalytic biofilm eradication.[44] In their work, supramolecular BCNs were synthesized by conjugating chlorin e6-/nitric oxide-modified α-cyclodextrin with a pH-sensitive copolymer. This BCN showed a negatively charged surface under physiological pH (≈7.4), making it stable in blood after injection, while under BME-typical acidic conditions (pH ≈ 5.5), the surface charge distribution of the BCNs switched to positive, promoting biofilm uptake. Upon the high concentration of GSH, the BCNs were reduced and released NO, which served as a GSH consumer just as it does in metabolic processes, as illustrated in Equation 1 (Figure 12B). Meanwhile, the depletion of GSH inevitably disequilibrated the redox system of bacterial cells and led to ROS accumulation, which in turn reinforced the PDT effects. Furthermore, GSH-triggered NO was able to further react with ROS generated during PDT, thus forming RNS to enhance bactericidal performance, as shown in Equation (2) (Figure 12B). This work provides a paradigm for the construction of pH- and GSH-dual responsive BCN systems with high BME-targeting accuracy.

3. Conclusion and Perspective

This review summarizes the most recent noteworthy progress in utilizing BCNs as a new pathway for bacterial disinfection. Empowered my growing insights into bacterial defense systems and biofilm formation mechanisms, numerous types of BCNs can destroy the bacterial cell membranes, inhibit bacterial colonization, disperse biofilms, and induce the BME-triggered toxicity. These studies have suggested innovative biocatalytic strategies for treating bacterial infection without giving rise to bacterial resistance. More significantly, BCNs exhibit various superior properties relative to immune cells and natural enzymes, such as higher biocatalytic performance, extraordinary stability against harsh conditions, adjustable composition, and production scalability. We anticipate that this review can provide new insights into developing BCNs as novel antibacterial agents for combating bacteria and biofilms and offer significant new inspiration for designing future biocatalytic nanoagents for clinical and industrial applications.

Even though we have seen the rapid development of disinfection-based BCNs in recent years, this nascent area faces several challenges and obstacles. From our perspective, these can be summarized as follows:

2100637 (17 of 21)

1) Most of the reported BCNs are mild and harmless toward healthy cells and tis sue, and only show on-demand toxicity under certain activation conditions—for instance, chemical auxiliaries, light irradiation, and sonification of BME. Nevertheless, as nanomaterials, their potential accumulative damage and carcinogenicity cannot be ignored. Especially for those therapeutics administered intravenously, the BCNs might tend to accumulate in the capillary-rich liver and spleen. These accumulated BCNs would first create an imbalance of ROS homeostasis, with the liver and spleen acting as the main targets of this increased oxidative stress. Afterward, the immune system would be aroused, and meanwhile, inflammatory cells would be activated for endocytosis against these foreign nanomaterials, even though they would not be able to successfully degrade and eliminate them. With the increasing amount of accumulated necrotic inflammatory cells, more severe outcomes like immune dysfunction, hepatocyte or splenocyte apoptosis, and hemangioma could occur. From our perspective, there are two promising directions to improve this situation. One is to further reduce the size of the nanomaterials to reduce their accumulation in the liver and spleen, and more importantly to enable them to leave the body via renal metabolism; another is to fabricate BCNs that can be gradually degraded in the physiological environment after treatment. It has been reported that various MOFs like Zn, Co-based ZIF, and Fe-based MOF series exhibit both catalytic performance and biodegradability, which endow them with remarkable potential for achieving degradable BCN-based therapy. Therefore, although there are few publications about biodegradable or renally clearable BCN-based antibacterial therapies, we expect to see more groundbreaking works that will overcome the existing challenges and promote the eventual clinical transformation of BCN-based therapy. Moreover, further boosting these BCNs' biocatalytic activities and targeted interactions with bacteria is essential to decreasing their required dosages, thus minimizing toxicity.

2) The detailed catalytic mechanisms of BCNs have been systematically studied in vitro. However, physiological conditions, are far more complicated than experimental simulations, and may tend to increase or reduce biocatalytic activities relative to in vitro observations. Unfortunately, we still lack the methods to monitor the catalytic process in vivo. Soon, with the improvement of characterization technologies, we expect more advanced strategies that can help provide researchers with an in-depth understanding of the catalytic modality under in situ physiological conditions.

3) To the best of our knowledge, there exist no reports confirming that bacteria have developed tolerance to ROS. As we look ahead to the long-term applications of ROS-based BCNs in antibacterial treatment, their potential for inducing resistance should be carefully examined for a long time.

4) Significant efforts have been made to endow BCNs with bacteria- and biofilm-targeting competence by using electrostatic interaction and pH- or GSH-responsiveness. But in biological conditions full of ions, buffers, proteins, and cells, the risk of missing the therapeutic target will be significantly increased, leading to low therapeutic efficacy and potential damage of healthy cells and tissues. Therefore, more accurate, tailor-made, and multifunctional bacteria- and biofilm-targeting BCN systems still need to be developed. Recent research has demonstrated that ROSs could act as inducers for localized macrophage-related immunity.[130] A combination of BME-targeted BCNs with immunotherapy might be a good future strategy for highly effective and accurate biofilm eradication.

5) We are still a long way off from translating BCNs into commonly used clinical antimicrobials. In terms of structure and catalytic mechanism, for nearly all kinds of BCNs, their metallic components serve as active sites for the catalytic process. With regard to the metal-based nanocomposites themselves, in addition to the accumulative toxicity that we mention above, future research and development must take into account the range of potential toxicities and pathogenicities threatened by ion leakage into the human body. Accordingly, BCNs with single-atomic metallic catalytic centers may be good candidates for clinical trials, since they maintain high catalytic activity while avoiding ion leakage.

6) Moreover, since BCNs can function as an excellent toolbox to combine and extend the advantages of other antibacterial modalities, researchers have constructed multifunctional BCN platforms with better bactericidal activity. Examples include endowing the BCNs with PTT, PDT, and SDT synergetic performance and coating them with unique spiky topography to penetrate bacterial outer structures or enhance interactions with bacteria.[11,131] However, in practical clinical treatment, these multifunctional platforms are not easy to achieve and will increase cost. Furthermore, to serve as viable alternatives to antibiotics, BCNs should also be able to reach unknown lesions and cure them via blood injections, a criterion that will be difficult for external tools like laser and sonification to fulfill. Future BCN designers should therefore give great attention to finding an appropriate balance between biocatalytic performance and clinical operability. In this rapidly evolving new field, we firmly expect that these problems will be solved in the near future, and that the use of BCNs in combating bacteria and biofilms will enable unprecedented medical progress.

Conflict of Interest

The authors declare no conflict of interest.

Author Contributions

X.F., L.M., C.C., and R.H. conceived the idea for this review. X.F., F.Y., and L.M. assisted with the figure layout and scheme design. X.F., F.Y., and C.X.N. discussed the manuscript structure and modified figures. L.M. composed the sono-responsive BCNs part, edited, and commented on the medically related discussions. X.F., L.M., C.C., and R.H. wrote and edited the manuscript. C.C. and R.H. supervised the whole project.

Keywords

[1] J. M. Blair, M. A. Webber, A. J. Baylay, D. O. Ogbolu, L. J. Piddock, *Nat. Rev. Microbiol.* **2015**, *13*, 42.

[2] Q. Yu, T. Deng, F.-C. Lin, B. Zhang, J. I. Zink, *ACS Nano* **2020**, *14*, 5926.

[3] F. Duan, X. Feng, Y. Jin, D. Liu, X. Yang, G. Zhou, D. Liu, Z. Li, X.-J. Liang, J. Zhang, *Biomaterials* **2017**, *144*, 155.

[4] M. Moghayedi, E. K. Goharshadi, K. Ghazvini, H. Ahmadzadeh, R. Ludwig, M. Namayandeh-Jorabchi, *Mater. Chem. Phys.* **2017**, *188*, 58.

[5] H. Song, Y. A. Nor, M. Yu, Y. Yang, J. Zhang, H. Zhang, C. Xu, N. Mitter, C. Yu, *J. Am. Chem. Soc.* **2016**, *138*, 6455.

[6] K. M. O'Connell, J. T. Hodgkinson, H. F. Sore, M. Welch, G. P. Salmond, D. R. Spring, *Angew. Chem., Int. Ed.* **2013**, *52*, 10706.

[7] M. Wegener, M. J. Hansen, A. J. Driessen, W. Szymanski, B. L. Feringa, *J. Am. Chem. Soc.* **2017**, *139*, 17979.

[8] A. Sirelkhatim, S. Mahmud, A. Seeni, N. H. M. Kaus, L. C. Ann, S. K. M. Bakhori, H. Hasan, D. Mohamad, *Nano-Micro Lett.* **2015**, *7*, 219.

[9] Z.-m. Xiu, Q.-b. Zhang, H. L. Puppala, V. L. Colvin, P. J. Alvarez, *Nano Lett.* **2012**, *12*, 4271.

[10] Y. Xia, X. Fan, H. Yang, L. Li, C. He, C. Cheng, R. Haag, *Small* **2020**, *16*, 2003010.

[11] C. Nie, L. Ma, H. Luo, J. Bao, C. Cheng, *Smart Mater. Med.* **2020**, *1*, 48.

[12] Y. Yang, X. Wu, C. He, J. Huang, S. Yin, M. Zhou, L. Ma, W. Zhao, L. Qiu, C. Cheng, C. Zhao, *ACS Appl. Mater. Interfaces* **2020**, *12*, 13698.

[13] C. Cheng, S. Li, A. Thomas, N. A. Kotov, R. Haag, *Chem. Rev.* **2017**, *117*, 1826.

[14] C. X. Nie, L. Ma, S. Li, X. Fan, Y. Yang, C. Cheng, W. F. Zhao, C. S. Zhao, *Nano Today* **2019**, *26*, 57.

[15] X. Fan, F. Yang, J. Huang, Y. Yang, C. Nie, W. Zhao, L. Ma, C. Cheng, C. Zhao, R. Haag, *Nano Lett.* **2019**, *19*, 5885.

[16] Y. Yang, Y. Deng, J. Huang, X. Fan, C. Cheng, C. Nie, L. Ma, W. Zhao, C. Zhao, *Adv. Funct. Mater.* **2019**, *29*, 1900143.

[17] G. Wang, H. Feng, L. Hu, W. Jin, Q. Hao, A. Gao, X. Peng, W. Li, K.-Y. Wong, H. Wang, *Nat. Commun.* **2018**, *9*, 2055.

[18] X. Fan, F. Yang, C. Nie, Y. Yang, H. Ji, C. He, C. Cheng, C. Zhao, *ACS Appl. Mater. Interfaces* **2018**, *10*, 296.

[19] Y. Yang, L. Ma, C. Cheng, Y. Deng, J. Huang, X. Fan, C. Nie, W. Zhao, C. Zhao, *Adv. Funct. Mater.* **2018**, *28*, 1705708.

[20] Z. Wang, T. Xia, S. Liu, *Nanoscale* **2015**, *7*, 7470.

[21] F. Vatansever, W. C. de Melo, P. Avci, D. Vecchio, M. Sadasivam, A. Gupta, R. Chandran, M. Karimi, N. A. Parizotto, R. Yin, *FEMS Microbiol. Rev.* **2013**, *37*, 955.

[22] Q. Tang, S. Cao, T. Ma, X. Xiang, H. Luo, P. Borovskikh, R. D. Rodriguez, Q. Guo, L. Qiu, C. Cheng, *Adv. Funct. Mater.* **2020**, *30*, 2007475.

[23] Y. Lin, J. Ren, X. Qu, *Acc. Chem. Res.* **2014**, *47*, 1097.

[24] H. Wei, E. Wang, *Chem. Soc. Rev.* **2013**, *42*, 6060.

[25] L. Jiao, H. Yan, Y. Wu, W. Gu, C. Zhu, D. Du, Y. Lin, *Angew. Chem., Int. Ed.* **2020**, *132*, 2585.

[26] Y. Hu, H. Cheng, X. Zhao, J. Wu, F. Muhammad, S. Lin, J. He, L. Zhou, C. Zhang, Y. Deng, *ACS Nano* **2017**, *11*, 5558.

[27] Z. Chen, Z. Wang, J. Ren, X. Qu, *Acc. Chem. Res.* **2018**, *51*, 789.

[28] B. Liu, Z. Huang, J. Liu, *Nanoscale* **2016**, *8*, 13562.

[29] X. Dai, Y. Zhao, Y. Yu, X. Chen, X. Wei, X. Zhang, C. Li, *ACS Appl. Mater. Interfaces* **2017**, *9*, 30470.

[30] Y. Zhu, J. Chen, S. Kaskel, *Angew. Chem., Int. Ed.* **2020**, *60*, 5010.

[31] J. Yang, Y. W. Yang, *Small* **2020**, *16*, 1906846.

[32] L. Zhang, J. Fischer, Y. Jia, X. Yan, W. Xu, X. Wang, J. Chen, D. Yang, H. Liu, L. Zhuang, M. Hankel, D. J. Searles, K. Huang, S. Feng, C. L. Brown, X. Yao, *J. Am. Chem. Soc.* **2018**, *140*, 10757.

[33] C. Fang, Z. Deng, G. Cao, Q. Chu, Y. Wu, X. Li, X. Peng, G. Han, *Adv. Funct. Mater.* **2020**, *30*, 1910085.

[34] S. Gao, H. Lin, H. Zhang, H. Yao, Y. Chen, J. Shi, *Adv. Sci.* **2019**, *6*, 1801733.

[35] Y. Jiang, X. Zhao, J. Huang, J. Li, P. K. Upputuri, H. Sun, X. Han, M. Pramanik, Y. Miao, H. Duan, *Nat. Commun.* **2020**, *11*, 1857.

[36] C. Yang, M. Zhou, C. He, Y. Gao, S. Li, X. Fan, Y. Lin, F. Cheng, P. Zhu, C. Cheng, *Nano-Micro Lett.* **2019**, *11*, 87.

[37] S. Liu, S. Cao, J. Guo, L. Luo, Y. Zhou, C. Lin, J. Shi, C. Fan, M. Lv, L. Wang, *Nanoscale* **2018**, *10*, 19603.

[38] Y. Seo, J. Hwang, E. Lee, Y. J. Kim, K. Lee, C. Park, Y. Choi, H. Jeon, J. Choi, *Nanoscale* **2018**, *10*, 15529.

[39] Q. Chen, D. Yang, L. Yu, X. Jing, Y. Chen, *Mater. Horiz.* **2020**, *7*, 317.

[40] Y. Tao, E. Ju, J. Ren, X. Qu, *Adv. Mater.* **2015**, *27*, 1097.

[41] X. He, F. Tian, J. Chang, X. Bai, C. Yuan, C. Wang, A. Neville, *ACS Sustainable Chem. Eng.* **2020**, *8*, 6744.

[42] C. Mao, Y. Xiang, X. Liu, Z. Cui, X. Yang, Z. Li, S. Zhu, Y. Zheng, K. W. K. Yeung, S. Wu, *ACS Nano* **2018**, *12*, 1747.

[43] Z. Liu, F. Wang, J. Ren, X. Qu, *Biomaterials* **2019**, *208*, 21.

[44] D. Hu, Y. Deng, F. Jia, Q. Jin, J. Ji, *ACS Nano* **2020**, *14*, 347.

[45] J. Gehring, B. Trepka, N. Klinkenberg, H. Bronner, D. Schleheck, S. Polarz, *J. Am. Chem. Soc.* **2016**, *138*, 3076.

[46] L. Ma, F. Jiang, X. Fan, L. Wang, C. He, M. Zhou, S. Li, H. Luo, C. Cheng, L. Qiu, *Adv. Mater.* **2020**, *32*, 2003065.

[47] W. Shao, C. He, M. Zhou, C. Yang, Y. Gao, S. Li, L. Ma, L. Qiu, C. Cheng, C. Zhao, *J. Mater. Chem. A* **2020**, *8*, 3168.

[48] W. Yin, J. Yu, F. Lv, L. Yan, L. R. Zheng, Z. Gu, Y. Zhao, *ACS Nano* **2016**, *10*, 11000.

[49] H. Ji, K. Dong, Z. Yan, C. Ding, Z. Chen, J. Ren, X. Qu, *Small* **2016**, *12*, 6200.

[50] J. Xi, G. Wei, L. An, Z. Xu, Z. Xu, L. Fan, L. Gao, *Nano Lett.* **2019**, *19*, 7645.

[51] F. Natalio, R. Andre, A. F. Hartog, B. Stoll, K. P. Jochum, R. Wever, W. Tremel, *Nat. Nanotechnol.* **2012**, *7*, 530.

[52] Z. Wang, K. Dong, Z. Liu, Y. Zhang, Z. Chen, H. Sun, J. Ren, X. Qu, *Biomaterials* **2017**, *113*, 145.

[53] X. Liu, Z. Yan, Y. Zhang, Z. Liu, Y. Sun, J. Ren, X. Qu, *ACS Nano* **2019**, *13*, 5222.

[54] A. Carvalho, M. Wang, X. Zhu, A. S. Rodin, H. Su, A. H. C. Neto, *Nat. Rev. Mater.* **2016**, *1*, 16061.

[55] J. Lu, J. Yang, A. Carvalho, H. Liu, Y. Lu, C. H. Sow, *Acc. Chem. Res.* **2016**, *49*, 1806.

[56] L. Jiao, Y. Wang, H. L. Jiang, Q. Xu, *Adv. Mater.* **2018**, *30*, 1703663.

[57] D. P. Cormode, L. Gao, H. Koo, *Trends Biotechnol.* **2018**, *36*, 15.

[58] Z. Chen, H. Ji, C. Liu, W. Bing, Z. Wang, X. Qu, *Angew. Chem., Int. Ed.* **2016**, *128*, 10890.

[59] Z. Ma, J. Li, Y. Bai, Y. Zhang, H. Sun, X. Zhang, *Chem. Eng. J.* **2020**, *399*, 125787.

[60] A. Gupta, R. Das, G. Yesilbag Tonga, T. Mizuhara, V. M. Rotello, *ACS Nano* **2018**, *12*, 89.

[61] Z. Yuan, C. Lin, Y. He, B. Tao, M. Chen, J. Zhang, P. Liu, K. Cai, *ACS Nano* **2020**, *14*, 3546.

[62] Y. Gao, J. Wang, M. Chai, X. Li, Y. Deng, Q. Jin, J. Ji, *ACS Nano* **2020**, *14*, 5686.

[63] Y. Liu, P. C. Naha, G. Hwang, D. Kim, Y. Huang, A. Simon-Soro, H. I. Jung, Z. Ren, Y. Li, S. Gubara, F. Alawi, D. Zero, A. T. Hara, D. P. Cormode, H. Koo, *Nat. Commun.* **2018**, *9*, 2920.

[64] D. Hu, H. Li, B. Wang, Z. Ye, W. Lei, F. Jia, Q. Jin, K.-F. Ren, J. Ji, *ACS Nano* **2017**, *11*, 9330.

[65] G. Fang, W. Li, X. Shen, J. M. Perez-Aguilar, Y. Chong, X. Gao, Z. Chai, C. Chen, C. Ge, R. Zhou, *Nat. Commun.* **2018**, *9*, 129.

[66] S. Cai, X. Jia, Q. Han, X. Yan, R. Yang, C. Wang, *Nano Res.* **2017**, *10*, 2056.

[67] S. Chen, Y. Quan, Y.-L. Yu, J.-H. Wang, *ACS Biomater. Sci. Eng.* **2017**, *3*, 313.

[68] J. Shan, X. Li, K. Yang, W. Xiu, Q. Wen, Y. Zhang, L. Yuwen, L. Weng, Z. Teng, L. Wang, *ACS Nano* **2019**, *13*, 13797.

[69] R. Li, N. D. Mansukhani, L. M. Guiney, Z. Ji, Y. Zhao, C. H. Chang, C. T. French, J. F. Miller, M. C. Hersam, A. E. Nel, *ACS Nano* **2016**, *10*, 10966.

[70] S. Huang, X. Kou, J. Shen, G. Chen, G. Ouyang, *Angew. Chem., Int. Ed.* **2020**, *59*, 8786.

[71] C. Wu, K. Schwibbert, K. Achazi, P. Landsberger, A. Gorbushina, R. Haag, *Biomacromolecules* **2017**, *18*, 210.

[72] Z. Zhao, Y. Huang, W. Liu, F. Ye, S. Zhao, *ACS Sustainable Chem. Eng.* **2020**, *8*, 4481.

[73] C. Zhang, L. Zhang, W. Wu, F. Gao, R.-Q. Li, W. Song, Z.-N. Zhuang, C.-J. Liu, X.-Z. Zhang, *Adv. Mater.* **2019**, *31*, 1901179.

[74] X. Yang, Y. Yang, F. Gao, J. J. Wei, C. G. Qian, M. J. Sun, *Nano Lett.* **2019**, *19*, 4334.

[75] N. Panwar, A. M. Soehartono, K. K. Chan, S. Zeng, G. Xu, J. Qu, P. Coquet, K.-T. Yong, X. Chen, *Chem. Rev.* **2019**, *119*, 9559.

[76] S. Dinda, S. Sarkar, P. K. Das, *Chem. Commun.* **2018**, *54*, 9929.

[77] C. Ge, R. Wu, Y. Chong, G. Fang, X. Jiang, Y. Pan, C. Chen, J. J. Yin, *Adv. Funct. Mater.* **2018**, *28*, 1801484.

[78] B. Xu, H. Wang, W. Wang, L. Gao, S. Li, X. Pan, H. Wang, H. Yang, X. Meng, Q. Wu, L. Zheng, S. Chen, X. Shi, K. Fan, X. Yan, H. Liu, *Angew. Chem., Int. Ed.* **2019**, *58*, 4911.

[79] T. Li, J. Li, Q. Pang, L. Ma, W. Tong, C. Gao, *ACS Appl. Mater. Interfaces* **2019**, *11*, 6789.

[80] X. Zhong, H. Xia, W. Huang, Z. Li, Y. Jiang, *Chem. Eng. J.* **2020**, *381*, 122758.

[81] Z. Chen, W. Gong, Z. Liu, S. Cong, Z. Zheng, Z. Wang, W. Zhang, J. Ma, H. Yu, G. Li, W. Lu, W. Ren, Z. Zhao, *Nano Energy* **2019**, *60*, 394.

[82] J. Wang, M. Bao, T. Wei, Z. Wang, Z. Dai, *Anal. Chim. Acta* **2020**, *1098*, 148.

[83] Z. Feng, X. Liu, L. Tan, Z. Cui, X. Yang, Z. Li, Y. Zheng, K. W. K. Yeung, S. Wu, *Small* **2018**, *14*, 1704347.

[84] C. Mao, Y. Xiang, X. Liu, Z. Cui, X. Yang, K. W. K. Yeung, H. Pan, X. Wang, P. K. Chu, S. Wu, *ACS Nano* **2017**, *11*, 9010.

[85] S. Liang, X. Deng, Y. Chang, C. Sun, S. Shao, Z. Xie, X. Xiao, P. Ma, H. Zhang, Z. Cheng, J. Lin, *Nano Lett.* **2019**, *19*, 4134.

[86] Y. Zhang, P. Sun, L. Zhang, Z. Wang, F. Wang, K. Dong, Z. Liu, J. Ren, X. Qu, *Adv. Funct. Mater.* **2019**, *29*, 1808594.

[87] P. Li, J. Li, X. Feng, J. Li, Y. Hao, J. Zhang, H. Wang, A. Yin, J. Zhou, X. Ma, B. Wang, *Nat. Commun.* **2019**, *10*, 2177.

[88] M. Huo, L. Wang, Y. Wang, Y. Chen, J. Shi, *ACS Nano* **2019**, *13*, 2643.

[89] L. Tan, J. Li, X. Liu, Z. Cui, X. Yang, S. Zhu, Z. Li, X. Yuan, Y. Zheng, K. W. K. Yeung, H. Pan, X. Wang, S. Wu, *Adv. Mater.* **2018**, *30*, 1801808.

[90] M. Huo, L. Wang, H. Zhang, L. Zhang, Y. Chen, J. Shi, *Small* **2019**, *15*, 1901834.

[91] Y. Sang, W. Li, H. Liu, L. Zhang, H. Wang, Z. Liu, J. Ren, X. Qu, *Adv. Funct. Mater.* **2019**, *29*, 1900518.

[92] J. Ouyang, R.-Y. Liu, W. Chen, Z. Liu, Q. Xu, K. Zeng, L. Deng, L. Shen, Y.-N. Liu, *J. Mater. Chem. B* **2018**, *6*, 6302.

[93] C. M. Courtney, S. M. Goodman, J. A. McDaniel, N. E. Madinger, A. Chatterjee, P. Nagpal, *Nat. Mater.* **2016**, *15*, 529.

[94] C. M. Courtney, S. M. Goodman, T. A. Nagy, M. Levy, P. Bhusal, N. E. Madinger, C. S. Detweiler, P. Nagpal, A. Chatterjee, *Sci. Adv.* **2017**, *3*, e1701776.

[95] Q. Gao, X. Zhang, W. Yin, D. Ma, C. Xie, L. Zheng, X. Dong, L. Mei, J. Yu, C. Wang, *Small* **2018**, *14*, 1802290.

[96] J. Hu, Q. Zhuang, Y. Wang, Y. Ni, *Analyst* **2016**, *141*, 1822.

[97] W. Fan, B. C. Yung, X. Chen, *Angew. Chem., Int. Ed.* **2018**, *57*, 8383.

[98] S.-S. Wan, J.-Y. Zeng, H. Cheng, X.-Z. Zhang, *Biomaterials* **2018**, *185*, 51.

[99] D. A. Wink, K. S. Kasprzak, C. M. Maragos, R. K. Elespuru, M. Misra, T. M. Dunams, T. A. Cebula, W. H. Koch, A. Andrews, J. S. Allen, *Science* **1991**, *254*, 1001.

[100] E. M. Hetrick, J. H. Shin, N. A. Stasko, C. B. Johnson, D. A. Wespe, E. Holmuhamedov, M. H. Schoenfisch, *ACS Nano* **2008**, *2*, 235.

[101] D. O. Schairer, J. S. Chouake, J. D. Nosanchuk, A. J. Friedman, *Virulence* **2012**, *3*, 271.

[102] D. Wang, L. Niu, Z.-Y. Qiao, D.-B. Cheng, J. Wang, Y. Zhong, F. Bai, H. Wang, H. Fan, *ACS Nano* **2018**, *12*, 3796.

[103] P. G. Wang, M. Xian, X. Tang, X. Wu, Z. Wen, T. Cai, A. J. Janczuk, *Chem. Rev.* **2002**, *102*, 1091.

[104] V. Calabrese, C. Mancuso, M. Calvani, E. Rizzarelli, D. A. Butterfield, A. M. G. Stella, *Nat. Rev. Neurosci.* **2007**, *8*, 766.

[105] X. Pang, Q. Xiao, Y. Cheng, E. Ren, L. Lian, Y. Zhang, H. Gao, X. Wang, W. Leung, X. Chen, *ACS Nano* **2019**, *13*, 2427.

[106] D. Sun, X. Pang, Y. Cheng, J. Ming, S. Xiang, C. Zhang, P. Lv, C. Chu, X. Chen, G. Liu, N. Zheng, *ACS Nano* **2020**, *14*, 2063.

[107] J. Ouyang, L. Deng, W. Chen, J. Sheng, Z. Liu, L. Wang, Y.-N. Liu, *Chem. Commun.* **2018**, *54*, 2874.

[108] J. Wang, L. Fang, P. Li, L. Ma, W. Na, C. Cheng, Y. Gu, D. Deng, *Nano-Micro Lett.* **2019**, *11*, 74.

[109] M. Whiteley, S. P. Diggle, E. P. Greenberg, *Nature* **2017**, *551*, 313.

[110] A. Butler, M. Sandy, *Nature* **2009**, *460*, 848.

[111] K. Herget, P. Hubach, S. Pusch, P. Deglmann, H. Götz, T. E. Gorelik, I. y. A. Gural'skiy, F. Pfitzner, T. Link, S. Schenk, *Adv. Mater.* **2017**, *29*, 1603823.

[112] M. Hu, K. Korschelt, M. Viel, N. Wiesmann, M. Kappl, J. Brieger, K. Landfester, H. Therien-Aubin, W. Tremel, *ACS Appl. Mater. Interfaces* **2018**, *10*, 44722.

[113] E. G. M. Vollenbroek, L. H. Simons, J. W. P. M. van Schijndel, P. Barnett, M. Balzar, H. Dekker, C. van der Linden, R. Wever, *Biochem. Soc. Trans.* **1995**, *23*, 267.

[114] H.-C. Flemming, J. Wingender, *Nat. Rev. Microbiol.* **2010**, *8*, 623.

[115] J. J. Swartjes, T. Das, S. Sharifi, G. Subbiahdoss, P. K. Sharma, B. P. Krom, H. J. Busscher, H. C. van der Mei, *Adv. Funct. Mater.* **2013**, *23*, 2843.

[116] C. Liu, Y. Zhao, W. Su, J. Chai, L. Xu, J. Cao, Y. Liu, *J. Mater. Chem. B* **2020**, *8*, 4395.

[117] M. Sun, L. Xu, A. Qu, P. Zhao, T. Hao, W. Ma, C. Hao, X. Wen, F. M. Colombari, A. F. de Moura, *Nat. Chem.* **2018**, *10*, 821.
[118] H. Ren, C. Wang, J. Zhang, X. Zhou, D. Xu, J. Zheng, S. Guo, J. Zhang, *ACS Nano* **2010**, *4*, 7169.
[119] C. Xu, X. Qu, *NPG Asia Mater.* **2014**, *6*, e90.
[120] F. Xu, Q. Lu, P. J. Huang, J. Liu, *Chem. Commun.* **2019**, *55*, 13215.
[121] Z. Ma, L. Wu, K. Han, H. Han, *Nanoscale Horiz.* **2019**, *4*, 1124.
[122] Z. Wang, Y. Zhang, E. Ju, Z. Liu, F. Cao, Z. Chen, J. Ren, X. Qu, *Nat. Commun.* **2018**, *9*, 3334.
[123] Y. Chen, H. Zhong, J. Wang, X. Wan, Y. Li, W. Pan, N. Li, B. Tang, *Chem. Sci.* **2019**, *10*, 5773.
[124] J. Mu, Y. Wang, M. Zhao, L. Zhang, *Chem. Commun.* **2012**, *48*, 2540.

[125] X. Hu, F. Li, F. Xia, X. Guo, N. Wang, L. Liang, B. Yang, K. Fan, X. Yan, D. Ling, *J. Am. Chem. Soc.* **2020**, *142*, 1636.
[126] W. Zhen, Y. Liu, L. Lin, J. Bai, X. Jia, H. Tian, X. Jiang, *Angew. Chem., Int. Ed.* **2018**, *130*, 10466.
[127] D. S. Benoit, H. Koo, *Nanomedicine* **2016**, *11*, 873.
[128] L. Gao, K. M. Giglio, J. L. Nelson, H. Sondermann, A. J. Travis, *Nanoscale* **2014**, *6*, 2588.
[129] Y. Deng, F. Jia, S. Chen, Z. Shen, Q. Jin, G. Fu, J. Ji, *Biomaterials* **2018**, *187*, 55.
[130] G. Guo, H. Zhang, H. Shen, C. Zhu, R. He, J. Tang, Y. Wang, X. Jiang, J. Wang, W. Bu, X. Zhang, *ACS Nano* **2020**, *14*, 13391.
[131] C. Nie, B. Parshad, S. Bhatia, C. Cheng, M. Stadtmüller, A. Oehrl, Y. Kerkhoff, T. Wolff, R. Haag, *Angew. Chem., Int. Ed.* **2020**, *59*, 15532.
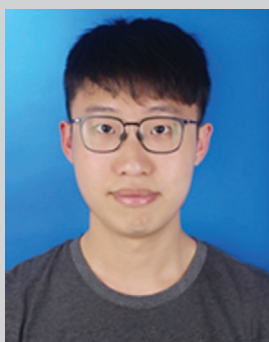
Xin Fan received his B.S. degrees from Hefei University of Technology, China in 2016. After obtaining his M.S. degree from Sichuan University, China in 2019, he became a Ph.D. candidate at Freie Universität Berlin in the group of Prof. Rainer Haag. His current research focuses on the design and fabrication of functional antibacterial and antibiofilm nanomaterials.

Chong Cheng is currently a full professor in the department of polymer science at Sichuan University. He obtained his B.Sc. and Ph.D. from Sichuan University. After a research stay at the University of Michigan, Ann Arbor, USA, he joined the Freie Universität Berlin as an AvH research fellow. His current scientific interests include fabricating advanced low-dimensional materials for nanomedicines, antibacterial materials, stem cell scaffolds, and electrocatalysts, especially the cutting-edge applications of metal-organic frameworks. He has published over 100 SCI papers, including Nature Materials, Science Advances, and Advanced Materials.

Rainer Haag is a full professor in macromolecular chemistry at the Freie Universität Berlin. Since 2021 he is the spokesperson of the Collaborative Research Center SFB 1449 "Dynamic Hydrogels at Biointerfaces". His research interests are dendritic polymers as highly functional polymeric supports, macromolecular nanotransporters for drug-delivery, and functional hydrogels at interfaces. Together with Dendropharm, he received the Berlin-Brandenburg Innovation Award 2016. Since 2019 he is an elected member of the German Academy of Science and Engineering (acatech). His scientific output is documented by >555 peer review publications and >35 patent applications. For more information see the group homepage: www.polytree.de.